Precambrian Research 381 (2022) 106848

Contents lists available at ScienceDirect

Precambrian Research

journal homepage: www.elsevier.com/locate/precamres

# Organic molecular evidence in the ~1.40 Ga Xiamaling Formation black shales in North China Craton for biological diversity and paleoenvironment of mid-Proterozoic ocean

Hong Xiao, Meijun Li [*], Tieguan Wang, Bing You, Xiaolin Lu, Xin Wang

*State Key Laboratory of Petroleum Resources and Prospecting, China University of Petroleum, Beijing 102249, China*
*College of Geosciences, China University of Petroleum, Beijing 102249, China*

ARTICLE INFO

*Keywords:*
Biomarkers
Eukaryotes
Biological diversity
Paleoenvironment
Proterozoic
North China Craton

ABSTRACT

Indigenous hydrocarbon biomarkers in the black shales of the 1.40 billion-year-old Xiamaling Formation (XML) from the North China Craton were systematically analyzed to reveal the redox condition and biological community. These black shales are not only rich in organic matter, but also undergone an unexpectedly low thermal evolution process, both of which contribute to well-preserved indigenous hydrocarbons and promote the convincing discovery of the Precambrian biology. The combination of the absence or low concentrations of gammacerane, dibenzothiophene series and aryl isoprenoids, abundant rearranged hopanes, the occurrence of micro-ripples, and low level of redox-sensitive trace elements suggested shallow, low salinity and suboxic to anoxic conditions during the deposition period of XML. The absence of aryl isoprenoids as diagnostic biomarkers for green/purple sulfur bacteria strongly argued against the pervasively euxinic (sulphidic) bottom water in mid-Proterozoic ocean. The scenario of large hump unresolved complex mixture and abundant monomethyl alkanes as well as absent steranes may be derived from benthic microbial reworking processes for biolipids. Here the absence of saturated and aromatic steroids in the XML sediments suggested that eukaryotic algae have little ecological contribution to primitive biomass and/or are the result of heterotrophic reworking from benthic microbial mats. Abundant presence of hopanoid, tricyclic terpane and *n*-alkane in these samples supported the predominant contribution of (cyano) bacteria.

## 1. Introduction

Anoxic and ferruginous conditions in the deep water of global marine basins during the 2.5–1.8 Ga period have been constructed and widely recognized (Holland, 1984). However, the understanding of ocean redox state of Earth's mid-Proterozoic (1.8–1.0 Ga), also known as "boring billion" (Holland, 2006), remains controversial but has been gradually developed (Holland, 1984; Canfield, 1998; Li et al., 2010; Poulton et al., 2010; Planavsky et al., 2011; Poulton and Canfield, 2011). The traditional views held that accumulation of dissolved oxygen in the ocean was responsible for the disappearance of banded iron formation (BIF) at 1.8 billion years ago (Holland, 1984), and then arose mildly oxidative conditions in both surface and deep oceans (Holland, 2006). Subsequently, Canfield (1998) proposed a sulphidic ocean model as an alternative model for the development of ocean chemistry of mid-Proterozoic ocean. The model mentioned that the early oxygenation facilitated the transport of terrestrial sulfates into the ocean and then formed abundant hydrogen sulfide for precipitation of dissolved Fe (II) as pyrite, which assumed that the mid-Proterozoic developed globally sulphidic (euxinic) deep ocean (Canfield, 1998). Moreover, the inorganic geochemical records (Shen et al., 2002; Poulton et al., 2004; Canfield, 2005) and lipid biomarkers (Brocks et al., 2005) provided abundant evidence for euxinic conditions, which further suggested that the euxinic ocean model may be applicable on a global scale and persisted into the Neoproterozoic until the second oxidation event in the Earth's surface environments (Canfield, 1998; Lyons et al., 2009).

More recently, contrary to previously popular model (Canfield, 1998), a detailed reconstruction of ocean redox structure was proposed by the method of iron–sulphur–carbon systematics for the Neoproterozoic Doushantuo Formation (635–542 Ma) in the Nanhua Basin, South China (Li et al., 2010) and the Mesoproterozoic Animikie Group (1.88–1.83 Ga) in the Superior region, North America (Poulton et al., 2010). These results revealed a stratified ocean with oxic conditions in surface water, euxinic (sulphidic) conditions in continental margin/

* Corresponding author.

https://doi.org/10.1016/j.precamres.2022.106848
Received 20 December 2021; Received in revised form 15 June 2022; Accepted 8 September 2022

shelf environments, and extensive anoxic and ferruginous (iron-rich) conditions in deep ocean (Li et al., 2010; Poulton and Canfield, 2011). Moreover, Planavsky et al. (2011) further analyzed the records of iron mineral speciation geochemistry and sulfur isotope of sulfides from diverse mid-Proterozoic basins, including the McArthur Basin that provided direct biomarker evidence for mid-Proterozoic euxinic conditions (Brocks et al., 2005). It further confirmed a widespread anoxic and ferruginous conditions in the mid-Proterozoic ocean (Planavsky et al., 2011), while the contemporaneous euxinic zones locally occurred in shallow continental shelf from lipid biomarker studies (Blumenberg et al., 2012; Nguyen et al., 2019; Cui et al., 2020). Accordingly, the apparent feature of the mid-Proterozoic seawater continuously remained globally anoxic and ferruginous conditions, rather than sulphidic (euxinic) (Planavsky et al., 2011; Poulton and Canfield, 2011).

It is well known that the redox chemistry of Earth's early ocean and the biological assemblage co-evolved. However, the earliest traces of eukaryotes and its evolution processes remain controversial (Rasmussen et al., 2008). As ancient phytoplankton rarely well-preserved as body fossil records in the Precambrian sediments, the molecular fossils of membrane lipids has opened up an effective complementary method for the convincing discovery of the Precambrian biology (Brocks et al., 2005; Bobrovskiy et al., 2018a; Bobrovskiy et al., 2018b), which is so-called "a molecular window to the primeval world" (Wang and Yuan, 2019). Careful analytical work has highlighted that rigorous analytical protocols and careful selection of unmetamorphosed samples are required to generate reliable data and to avoid detecting younger biomarker contaminants in Precambrian rocks (Sherman et al., 2007; Rasmussen et al., 2008; Brocks, 2011; Nguyen et al., 2019; Ai et al., 2020). Consequently, previous results on the timing of emergence and evolution of eukaryotes in early ocean have gradually been questioned and then reassessed (Brocks et al., 1999; Rasmussen et al., 2008). Globally, there are only a few localities that can offer the valuable and reliable Precambrian biomarker information, especially the Mesoproterozoic or older sequences, which emphasizes the necessity of additional work on various Precambrian sedimentary environments.

The ~1.40 Ga Xiamaling Formation (XML) in the North China Craton (NCC) developed exceptionally well-preserved organic-rich shales with low maturity (Wang et al., 2018), which is unique superiority in the study of biomarker compositions in early Earth. Here we reported the distinctive hydrocarbon biomarkers of the XML black shales in the NCC. The results of this study offer convincing evidence for the authenticity of the biological assemblage and paleoenvironment, which is a prerequisite for preserving diagnostic biomarker information in ancient rocks and oils.

## 2. Geological setting

The North China Craton deposits a set of discontinuous sequences of the Proterozoic to the Cenozoic, which contains a series of marine carbonate-clastic sequences with the thickness of up to 10 km during the Proterozoic Eon (Sun and Wang, 2016). Recently, high-precision zircon dating for bentonite layer within the Xiamaling Formation in the Xuanhua areas yielded an age of 1392.2 ± 1.0 Ma (Zhang et al., 2015; Zhang et al., 2016). During the deposition period of Xiamaling Formation, the depocenter shifted westwards to the Xuanlong Depression from the Jibei Depression in the NCC (Fig. 1a). The Xiahuayuan section (XHY) located in Zhangjiakou city of Hebei province (Fig. 1a), as a typical representative field outcrop section, well develops the Xiamaling Formation sequence with a total sedimentary thickness of up to 500 m.

Generally, the Xiamaling Formation is considered to be deposited in the estuary to restricted gulf depositional environments (Yan and Liu, 1998), and it consists of four lithological members (Fig. 1b). The Member 1 and Member 2 were deposited in shallow supratidal to subtidal zones with a thickness of approximately 160 m (Fig. 1b), which is mainly composed of purple-red shales, gray-green shales, brown sandstones, and emerald green sandstones. During the sedimentary period of the Member 3, the sea level in the NCC rose significantly and the paleowater depth became sharply deeper than the Member 1 and Member 2 (Fig. 1b). As the thickest member of the Xiamaling Formation (~350 m), in addition to the gray-green and gray shale beds, the Member 3 develops a bed of low-mature black shale/oil shale with high abundance of organic matter (Fig. 1b). The Member 4 consists of stromatolite limestone of the lower part, the gray-green shale, siliceous rock and gray dolomite nodules of the middle part, and the gray-black shale and siliceous rock of the upper part (Fig. 1b) (Zhang et al., 2007).

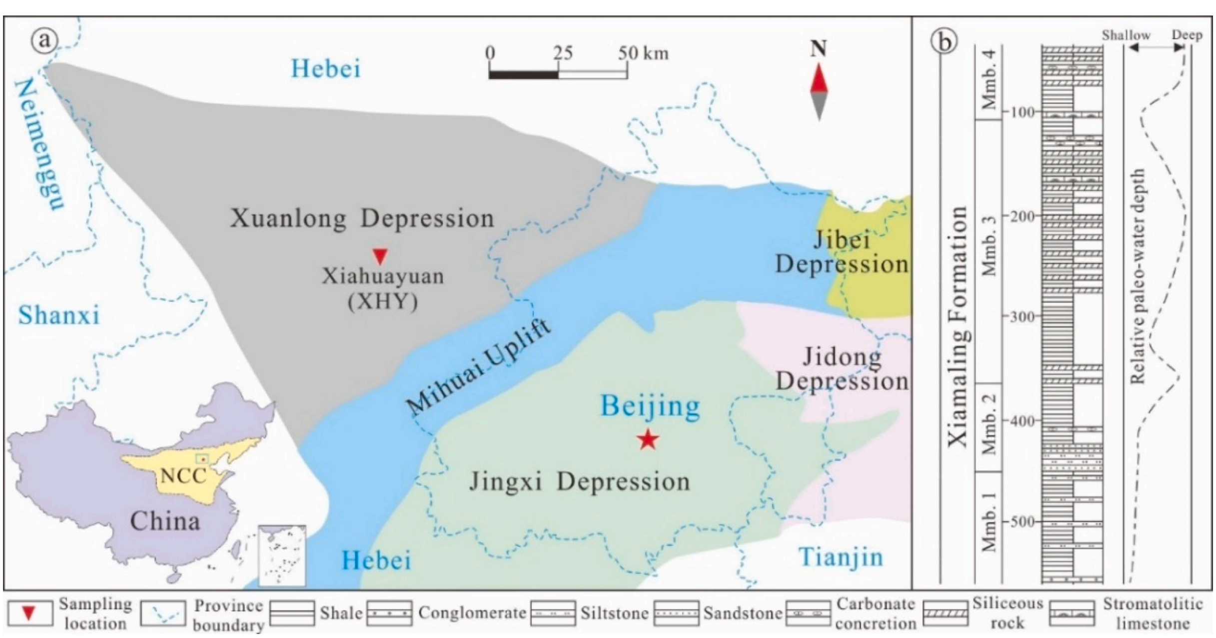


**Fig. 1.** Sampling location (a) and schematic stratigraphic column of the Xiamaling Formation (b) in the Xiahuayuan district (XHY), Zhangjiakou city, Hebei province, China.

## 3. Sampling and experiments

### 3.1. Rock samples

Nine black shale samples were collected from the Member 3 of the Xiamaling Formation in the Xiahuayuan section (Fig. 1a). All samples were collected after removing covered vegetation and oxidized surface rocks (Fig. 2a), so that they are fresh and have no ferric oxide stains in their surface (Fig. 2c-d). Interestingly, some samples are readily ignitable because of their extremely high content of organic matter (Fig. 2b). The abundance, type and maturity of organic matter were determined by the analysis data of total organic carbon and Rock-Eval pyrolysis, and all detailed data were listed in Table 1.

### 3.2. Soluble hydrocarbon extraction and fractionation

The soluble organic matter of nine shales were extracted from more than 100 g ground samples by Soxhlet apparatus for 72 h. The extracts were concentrated by a rotary evaporator, and then dissolved with 40–50 ml petroleum ether in a precleaned glass container, followed by using $N_2$ stream to reduce of the solvent to nearly dry. The resulting extracts filtered by a funnel stuffed to remove insoluble asphaltenes (F1). The residual solution can be further separated into saturated fraction (F2), aromatic fraction (F3) and resin fraction (F4) through a chromatography column through filled with dry silica gel and alumina. F2 fraction was isolated with redistilled petroleum ether as eluent, F3 fraction with mixed reagent of redistilled dichloromethane and redistilled petroleum ether (2:1, v/v), and F4 fraction with mixed reagent of redistilled dichloromethane and redistilled methanol (93:7, v/v).

### 3.3. Gas chromatography-mass spectrometry

Saturated and aromatic fractions were conducted by gas chromatography-mass spectrometry (GC–MS) to determine molecular marker compositions. The analytical instrument of GC–MS is composed of an Agilent 6890 gas chromatograph and Agilent 5975i mass spectrometer. The HP-5 MS fused silica capillary column was equipped in GC instrument, and the Helium was used as carries gas. The MS source was operated in electron impact with ionization energy of 70 eV and a scanning range of 50–600 Da. For saturated hydrocarbon, the oven temperature was initially set at 50 °C and kept for 1 min, then increased to 120 °C at 20 °C/min, finally to 310 °C at 3 °C/min and kept for 25 min. For the aromatic hydrocarbon, the oven temperature was also set at 50 °C and kept for 1 min, and then programmed to 310 °C at 3 °C/min and kept for 16 min.

### 3.4. Gas chromatography–mass spectrometry-mass spectrometry

The gas chromatography–mass spectrometry–mass spectrometry (GC–MS–MS) technique was applied to detect 13α(*n*-alkyl)-tricyclic terpanes and rearranged hopanes in saturated fraction. GC–MS–MS analysis was performed on an Agilent 6890 Series gas chromatograph coupled to a Quatro II mass spectrometer. The oven temperature was initially set at 50 °C and kept for 1 min, and then programmed to 120 °C at 20 °C/min, and then continue to rise to 250 °C at 4 °C/min and 310 °C at 3 °C/min, finally kept for 30 min. The MS source was operated in electron impact with ionization energy of 70 eV. The Helium was used as carries gas with a constant flow of 1 ml/min.

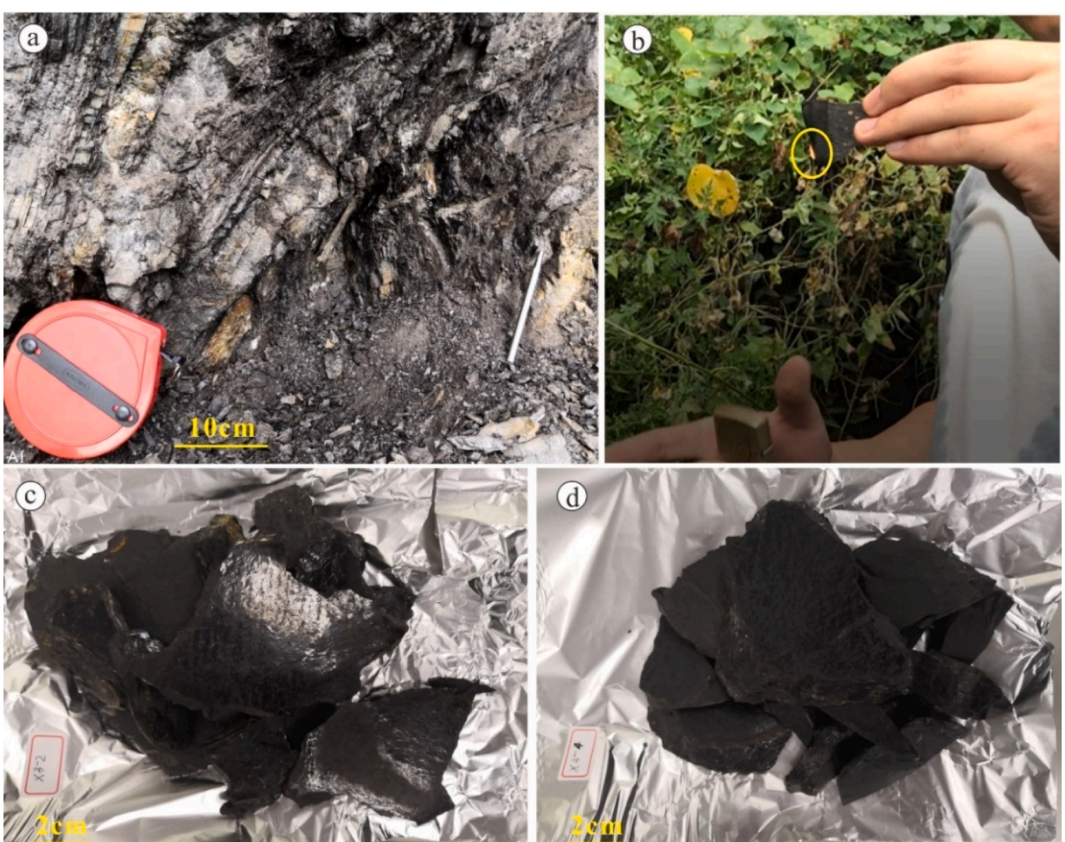


**Fig. 2.** Generalized features of black shales of the Xiamaling Formation. (a) the outcrop of black shales of Xiamaling Formation in the Xiahuayuan area (XHY), Hebei province. A pickaxe was used to remove vegetation and oxidized layers on the surface, then exposing fresh rocks; (b) ignition of the black shales; (c-d) the outcrop samples of black shales collected from XHY section depicting organic-rich layers.

**Table 1**
Geochemical data of black shales from the Xiamaling Formation in the study.

| Sample | Formation | Lithology | $S_1$ (mg/g) | $S_2$ (mg/g) | Tmax (°C) | $S_1 + S_2$ (mg/g) | TOC (%) | HI (mg/g) |
|---|---|---|---|---|---|---|---|---|
| XHY_1 | Xiamaling | Black shale | 0.43 | 25.24 | 434 | 25.67 | 6.43 | 392.35 |
| XHY_2 | Xiamaling | Black shale | 1.35 | 64.67 | 438 | 66.02 | 12.10 | 534.46 |
| XHY_3 | Xiamaling | Black shale | 0.59 | 35.61 | 442 | 36.20 | 7.36 | 483.83 |
| XHY_4 | Xiamaling | Black shale | 1.74 | 55.10 | 436 | 56.84 | 12.59 | 437.65 |
| XHY_5 | Xiamaling | Black shale | 1.23 | 11.08 | 434 | 12.31 | 2.20 | 503.41 |
| XHY_6 | Xiamaling | Black shale | 0.59 | 2.92 | 435 | 3.51 | 1.51 | 192.88 |
| XHY_7 | Xiamaling | Black shale | 0.14 | 12.66 | 438 | 12.80 | 4.16 | 304.62 |
| XHY_8 | Xiamaling | Black shale | 0.25 | 9.80 | 436 | 10.05 | 3.46 | 283.16 |
| XHY_9 | Xiamaling | Black shale | 0.20 | 16.41 | 436 | 16.61 | 4.56 | 360.11 |

## 4. Results

### 4.1. Bulk geochemical characteristics

The detailed data of organic carbon content (TOC) and rock–eval pyrolysis were shown in Table 1. These black shale samples have very high TOC contents in the range of 1.51–12.59 % with the averaged value of 6.04 % (Table 1). Temperature at maximum generation of rock–eval pyrolysis (Tmax, °C) shows obviously low values with the value range of 434–442 °C, but the hydrogen index (HI, mg HC/g TOC) is in the range of 192.88–534.46 mg/g (Table 1). Genetic potential ($S_1 + S_2$, mg/g) is in the range of 3.51–66.02 mg/g with a high averaged value of 26.67 mg/g (Table 1). In the cross-plots of $S_1 + S_2$ and TOC (Robison et al., 1999), eight of nine samples are distributed in the area of the excellent source rock, and the remaining one sample also falls into good source rock (Fig. 3a). The cross-plot of HI and Tmax for kerogen type classification (Mukhopadhyay et al., 1995) illustrates that all samples belong to Type $II_1$–$II_2$ kerogen (Fig. 3b).

In the extracted material, the percentages of saturated and aromatic fractions show relatively low values with the range of 12.3–50.0 % and 12.4–25.3 %, respectively (Table 2). While the proportion of non-hydrocarbons containing resins and asphaltenes is relatively high with an average value up to 60.6 % (Table 2).

### 4.2. Microscope observation

Microfacies observation revealed the layered distribution of organic matter without identifiable pyrite (Fig. 4). The organic matter was not strongly disturbed after deposition and present ripple-like structural occurrences, which is an obvious signature of the origin of the cyanobacteria mats. It is proposed that the organic-rich layer was formed by in-situ burial of benthic microbial mats in subtidal zone (Wang and Li, 1993; Tian, 1996). In addition, a large amount of fine siliciclastic material is concentrated in the micro-ripples and covered by early microbial mats (Fig. 4a-b). The micro-ripples are generally deposit above wave base, indicating that the depositional environment is shallow condition of intertidal to subtidal zones (Blumenberg et al., 2012; Miao et al., 2021).

Maceral compositions of the Xiamaling Formation black shale mainly consists of mineral-bituminous groundmass, protobitumen, and lamalginite (Fig. 4c-f). Among them, the mineral-bituminous groundmass is defined as a substance composed of submicroscopic organic matter and minerals (Teichmuller, 1988). It is conceivable that the identification of the organic matter compositions in mineral-bituminous groundmass is difficult to achieve, but which always exhibits strong fluorescence characteristics (Fig. 4f). The protobitumen, as another maceral component, is considered to be formed by autochthonous bitumen (Alpern, 1980), which was the dominant component of maceral in the Xiamaling Formation shales, with a maximum of ~40 vol% (Fig. 4e-f).

Moreover, the protobitumen always extends parallel to the bedding and interbeds with the mineral-bituminous groundmass (Fig. 4e), but has no fluorescence (Fig. 4f). Alpern (1980) proposed that because the protobitumen has the characteristics of *syn*-sedimentary and autochthonous origin, its reflectance can be effectively used for maturity evaluation, especially for some geological samples lacking vitrinite. In the study, the value of protobitumen reflectance is in the ranges of 0.46–0.49 % for our samples (Table 5), and further converted into equivalent vitrinite reflectance values (Jacob, 1989). Interestingly, the protobitumen was also proposed to be formed by microbial degradation of the lipidic components during sinking slowly process of organic material in the water column (Alpern, 1980), which was also observed in the Hongshuizhuang Formation (~1.45 Ga) in NCC (Luo et al., 2014) and the Roper Group in the McArthur Basin (Crick, 1992).

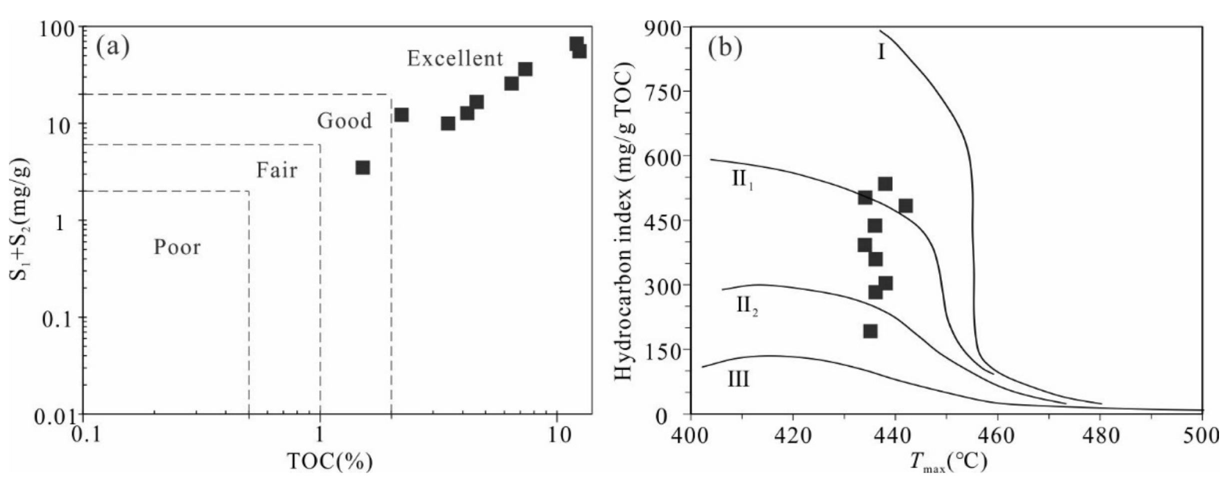


**Fig. 3.** Variation of $S_1 + S_2$ value with TOC content (a) and HI with Tmax (b) for black shales of the Xiamaling Formation showing genetic potential, kerogen type and thermal maturity.

**Table 2**
The weight of the samples used for extraction and relative percentage of soluble hydrocarbon components.

| Sample | Formation | Lithology | Samples (mg) | Saturates (%) | Aromatics (%) | Resins (%) | Asphaltenes (%) | Non-hydrocarbon (%) | Saturates/ Aromatics |
|---|---|---|---|---|---|---|---|---|---|
| XHY_1 | Xiamaling | Black shale | 49.55 | 14.8 | 12.4 | 24.4 | 48.4 | 72.8 | 1.20 |
| XHY_2 | Xiamaling | Black shale | 33.60 | 14.8 | 14.8 | 10.9 | 59.5 | 70.4 | 1.00 |
| XHY_3 | Xiamaling | Black shale | 36.05 | 12.3 | 22.3 | 33.5 | 31.9 | 65.4 | 0.55 |
| XHY_4 | Xiamaling | Black shale | 36.80 | 20.0 | 12.6 | 31.8 | 35.5 | 67.4 | 1.58 |
| XHY_5 | Xiamaling | Black shale | 34.30 | 25.6 | 17.2 | 41.0 | 16.1 | 57.1 | 1.49 |
| XHY_6 | Xiamaling | Black shale | 31.50 | 50.0 | 19.8 | 17.8 | 12.4 | 30.2 | 2.52 |
| XHY_7 | Xiamaling | Black shale | 33.00 | 26.7 | 25.3 | 27.6 | 20.4 | 48.0 | 1.06 |
| XHY_8 | Xiamaling | Black shale | 33.15 | 18.8 | 15.8 | 22.5 | 42.9 | 65.4 | 1.19 |
| XHY_9 | Xiamaling | Black shale | 33.00 | 15.3 | 15.8 | 18.2 | 50.7 | 68.9 | 0.97 |

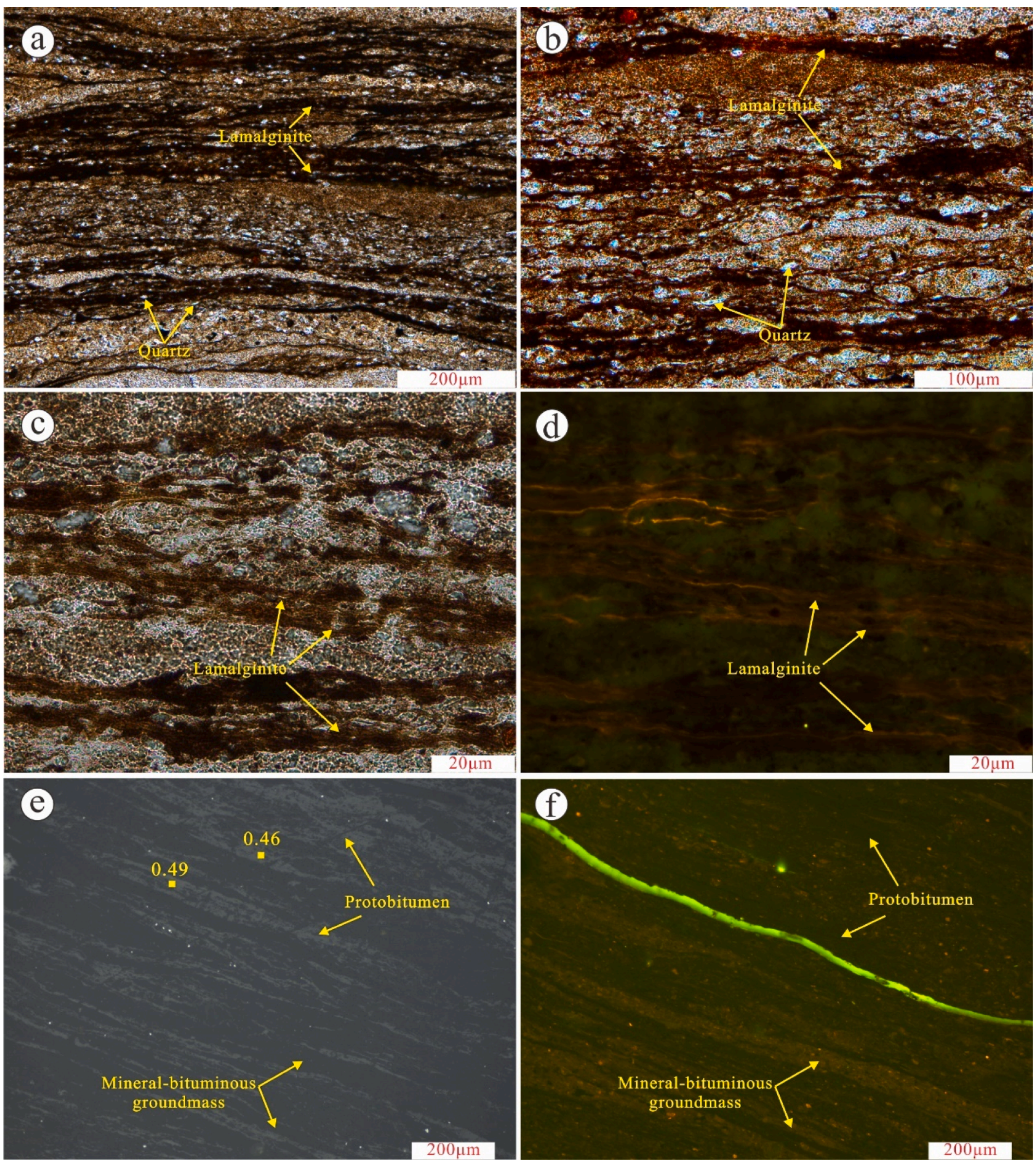


**Fig. 4.** Photomicrograph of the Xiamaling Formation black shale (XHY_1). (a-b) transmitted light, illustrating strata of microbial mats; (c) transmitted light, showing the lamalginite; (d) the same filed as (c), but in a fluorescence mode; (e) reflectance light, showing the protobitumen and mineral-bituminous groundmass; (f) the same filed as (e), but in a fluorescence mode. Note: the yellow squares represent the measurement points.

### 4.3. Saturated hydrocarbons

#### 4.3.1. Total ion chromatogram of saturated hydrocarbon

All samples show similar distribution pattern of normal alkanes (*n*-alkanes) in the total ion chromatogram (TIC) of saturated hydrocarbon. In the Fig. 5, there is not only contain a complete distribution of *n*-alkanes, but also exhibit a pronounced hump of baseline (unresolved complex mixture, UCM) (Fig. 5). The carbon number range of *n*-alkanes

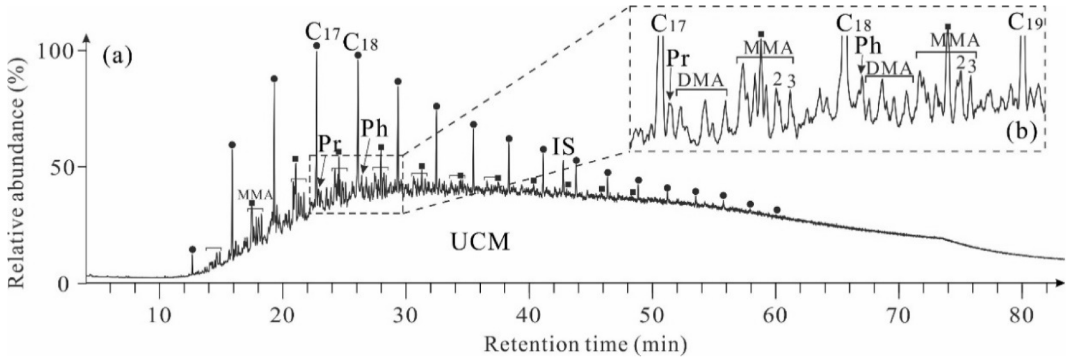


**Fig. 5.** Representative total ion chromatogram of saturated hydrocarbon of the black shale from the Xiamaling Formation. Notes: solid circles = normal alkanes; solid squares = *n*-alkylcyclohexanes; IS = internal standard; MMA = monomethyl alkanes; DMA = dimethyl alkanes; UCM = unresolved complex mixture.

is from $C_{14}$ to $C_{32}$, exhibiting a unimodal distribution pattern with a strong predominance of low-molecular-weight *n*-alkanes (maxima at $C_{17}$ or $C_{18}$) (Fig. 5, Table 3). Moreover, $nC_{21-}/nC_{22+}$ values are higher than 1.22 with the average value of 2.23 (Table 3), revealing the abundance advantage of low-carbon *n*-alkanes (Fig. 5). Obvious odd-to-even preference and high carbon preference usually occurs in low-mature samples with dominated inputs of terrestrial organic matter, which was not observed in our study as expected from bitumen of such old samples.

Acyclic isoprene alkanes such as pristane and phytane were detected with relative low abundance (Fig. 5), whereas the higher carbon number of $C_{21}$ + regular isoprenoids usually derived from ether-bound membrane lipids of halophilic archaea (Grice et al., 1998) were not observed. The values of pristane to phytane ratio (Pr/Ph) are in the range of 0.75–0.91. The value ranges of $Pr/nC_{17}$ (0.08–0.18) and $Ph/nC_{18}$ (0.09–0.19) ratios of the Xiamaling black shale (Table 3) are significantly lower than that of the black shales from the 1.1 Ga Touirist Formation (Blumenberg et al., 2012) and the 1.64 Ga Barney Creek Formation (Brocks et al., 2005), but similar to some Mesoproterozoic sediments from the McMinn, Velkerri formations in the McArthur Basin (Summons et al., 1988b).

The *n*-alkylcyclohexane series show similar distribution patterns with *n*-alkanes, but has slightly higher carbon number as major peak (e.g. *n*-alkylcyclohexane at $C_{18}$ vs *n*-alkanes at $C_{17}$ in Fig. 5). In addition, all samples contain abundant monomethyl alkanes (MMA) (Fig. 5b), the same as prevalent UCM, both of which seem to be typical characteristic of Proterozoic bitumen (Pawlowska et al., 2013).

### 4.3.2. Cheilanthanes and $C_{24}$ tetracyclic terpane

In the mass chromatogram *m/z* 191, a series of $C_{19}$–$C_{26}$ 13β(H),14α(H)-tricyclic terpanes ($C_{19}$–$C_{26}$TT), also namely cheilanthanes, were detected (Fig. 6). Although these samples are still in the low-mature thermal evolution stage (Table 1), the TT series in some samples have slight advantage in relative abundance over hopane series (Fig. 6a). Generally, the short-chain tricyclic terpenes ($C_{19}$–$C_{20}$TT) were usually enriched in coal-bearing strata and the source rocks with predominant inputs of terrestrial higher plants (Aquino Neto et al., 1982; Zumberge, 1987; Xiao et al., 2019c). Interestingly, in these mid-Proterozoic sediments, major homologue among $C_{19}$–$C_{29}$TT is the $C_{19}$ or $C_{20}$ short-chain tricyclic terpene (Fig. 6b). The similar scenarios were also observed in the Archean bitumen of the Hamersley Group in the Pilbara Craton (Western Australia) (Brocks et al., 2003a) and the Mesoproterozoic sediments from the Taoudeni Basin (northwestern Africa) (Blumenberg et al., 2012). The value of $C_{19+20}$TT to $C_{23}$TT ratio ($C_{19+20}/C_{23}$TT ratio) ranges from 2.73 to 17.23 with an extremely high average value of 8.22 (Table 4). Moreover, the relative percentage of $C_{19}$–$C_{23}$ tricyclic terpenes were further calculated, and the results showed that the average percentages of $C_{19+20}$TT, $C_{21}$TT and $C_{23}$TT tricyclic terpenes in analyzed samples were 74.15 %, 14.02 %, and 11.83 %, respectively (Table 4). The values of $C_{26}/C_{25}$TT ratio are less than 1.0 with the range of 0.63–0.86 (Table 4), indicating the marine sedimentary environment (Zumberge, 1987; Peters et al., 2005).

In addition, a $C_{24}$ tetracyclic terpane ($C_{24}$Tet, $M^+$ 330), also namely 17,21-*seco*hopane ($C_{24}$) (Aquino Neto et al., 1983), was also abundantly distributed in our samples (Fig. 6b). The value of $C_{24}$Tet to $C_{26}$TT ratio ($C_{24}$Tet/$C_{26}$TT) ranges from 1.95 to 5.95 with a high average value of 3.85 (Table 4). Such high values of $C_{24}$Tet/$C_{26}$TT was also reported in the Mesoproterozoic sediments from the Taoudeni Basin (Blumenberg et al., 2012).

### 4.3.3. Regular hopanes and rearranged hopanes

The carbon number distribution of regular hopanes (abbreviated as H series) are typically comprised of $C_{27}$ and $C_{29}$–$C_{35}$ homologues. $C_{30}$H is always the dominant homologue in H series, while the relative concentration of $C_{31}$–$C_{35}$ homohopanes gradually decreases with extremely low values of $C_{35}$ homohopane index ($C_{35}/(C_{31}$–$C_{35})$ homohopanes) (Fig. 7a). The thermal maturity indicators of 22S/(22S + 22R) ratios are in the value ranges of 0.55–0.58 (Table 4). Gammacerane (Ga) was firstly detected in the Green River shale (Hills et al., 1966) and usually used to characterize water column stratification environment as a result of hypersaline condition (Peters and Moldowan, 1993). In the study,

**Table 3**
Biomarker parameters calculated from total ion chromatogram of saturated hydrocarbon of the Xiamaling Formation black shales.

| Sample | Formation | Lithology | Pr/Ph | $Pr/nC_{17}$ | $Ph/nC_{18}$ | $Ph/nC_{18}$-$Pr/nC_{17}$ | $nC_{21}$-/ $nC_{22}$+ | CPI | OEP | Max. peak |
|---|---|---|---|---|---|---|---|---|---|---|
| XHY_1 | Xiamaling | black shale | 0.87 | 0.25 | 0.26 | 0.01 | 1.22 | 1.07 | 0.86 | C18 |
| XHY_2 | Xiamaling | black shale | 0.78 | 0.25 | 0.28 | 0.03 | 1.26 | 1.12 | 1.01 | C17 |
| XHY_3 | Xiamaling | black shale | 0.91 | 0.26 | 0.29 | 0.03 | 1.33 | 1.11 | 0.92 | C18 |
| XHY_4 | Xiamaling | black shale | 0.75 | 0.18 | 0.19 | 0.01 | 1.52 | 1.10 | 0.91 | C18 |
| XHY_5 | Xiamaling | black shale | 0.85 | 0.13 | 0.18 | 0.05 | 4.69 | 1.19 | 0.93 | C17 |
| XHY_6 | Xiamaling | black shale | 0.89 | 0.08 | 0.09 | 0.01 | 1.75 | 0.99 | 1.02 | C17 |
| XHY_7 | Xiamaling | black shale | 0.89 | 0.14 | 0.18 | 0.04 | 3.56 | 1.10 | 0.95 | C17 |
| XHY_8 | Xiamaling | black shale | 0.88 | 0.14 | 0.16 | 0.02 | 2.44 | 1.11 | 0.94 | C17 |
| XHY_9 | Xiamaling | black shale | 0.90 | 0.14 | 0.16 | 0.02 | 2.26 | 1.19 | 0.90 | C17 |

Note: CPI: carbon preference index; OEP: odd–even predominance; $C_{21}$-/$C_{22}$+: $C_{21}$- normal alkanes/$C_{22}$ + normal alkanes ratio; $Pr/nC_{17}$: pristine/$nC_{17}$ alkane ratio; $Ph/nC_{18}$: phytane/$nC_{18}$ alkane ratio; Pr/Ph: pristine/phytane ratio.

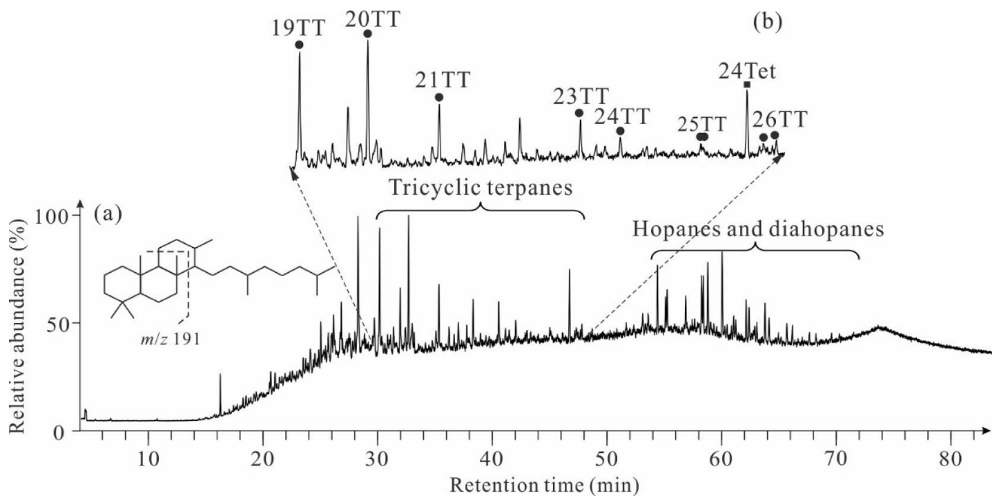


**Fig. 6.** Representative $m/z$ 191 mass chromatogram showing the distribution of regular tricyclic terpanes, regular hopanes and diahopanes in the saturated hydrocarbon of black shale from the Xiamaling Formation. Notes: 19TT-26TT = $C_{19}$-$C_{26}$ tricyclic terpanes; 24Tet = $C_{24}$ tetracyclic terpane.

**Table 4**
Biomarker parameters of saturated hydrocarbons of black shales from the Xiamaling Formation in the North China Craton.

| Sample | $C_{19+20}$TT (%) | $C_{21}$TT (%) | $C_{23}$TT (%) | $C_{19+20}$/$C_{23}$TT | $C_{24}$Tet/$C_{26}$TT | $C_{19}$αNATT/$C_{30}$H | Ga/$C_{30}$H | $C_{30}$E/$C_{30}$H | $C_{30}$D/$C_{30}$H | $C_{29}$Nsp/$C_{29}$H | $C_{29}$Ts/$C_{29}$H | $C_{31}$H 22S/(22S + 22R) | $C_{32}$H 22S/(22S + 22R) | 2-MHI | $C_{26}$/$C_{25}$TT |
|---|---|---|---|---|---|---|---|---|---|---|---|---|---|---|---|
| XHY_1 | 80.28 | 9.77 | 9.95 | 8.07 | 4.25 | 2.95 | 0.06 | 0.23 | 0.62 | 0.31 | 1.15 | 0.58 | 0.57 | 0.038 | 0.83 |
| XHY_2 | 79.59 | 11.45 | 8.95 | 8.89 | 4.27 | 3.48 | 0.06 | 0.21 | 0.61 | 0.31 | 1.08 | 0.58 | 0.56 | 0.029 | 0.63 |
| XHY_3 | 87.23 | 7.70 | 5.06 | 17.23 | 4.88 | 2.51 | 0.05 | 0.15 | 0.46 | 0.30 | 1.00 | 0.57 | 0.56 | 0.032 | 0.86 |
| XHY_4 | 87.93 | 6.89 | 5.18 | 16.97 | 5.95 | 5.39 | 0.05 | 0.16 | 0.48 | 0.22 | 0.88 | 0.58 | 0.57 | – | – |
| XHY_5 | 67.89 | 17.60 | 14.51 | 4.68 | 4.58 | 9.21 | 0.06 | 0.26 | 0.67 | 0.38 | 1.17 | 0.55 | 0.56 | – | – |
| XHY_6 | 59.74 | 18.40 | 21.86 | 2.73 | 2.79 | 7.40 | 0.08 | 0.33 | 0.44 | 0.23 | 0.73 | 0.55 | 0.57 | – | – |
| XHY_7 | 72.57 | 15.19 | 12.24 | 5.93 | 3.86 | 15.17 | 0.06 | 0.40 | 0.88 | 0.28 | 1.02 | 0.58 | 0.57 | – | – |
| XHY_8 | 68.49 | 19.14 | 12.37 | 5.54 | 2.14 | 5.46 | 0.08 | 0.27 | 0.64 | 0.34 | 0.96 | 0.56 | 0.58 | – | – |
| XHY_9 | 63.64 | 20.06 | 16.31 | 3.90 | 1.95 | 4.83 | 0.08 | 0.17 | 0.37 | 0.22 | 0.68 | 0.55 | 0.58 | – | – |

Note: 2-MHI = $C_{31}$ 2α-methylhopane/($C_{31}$ 2α-methylhopane + $C_{30}$ hopane) ; '-' = no data.

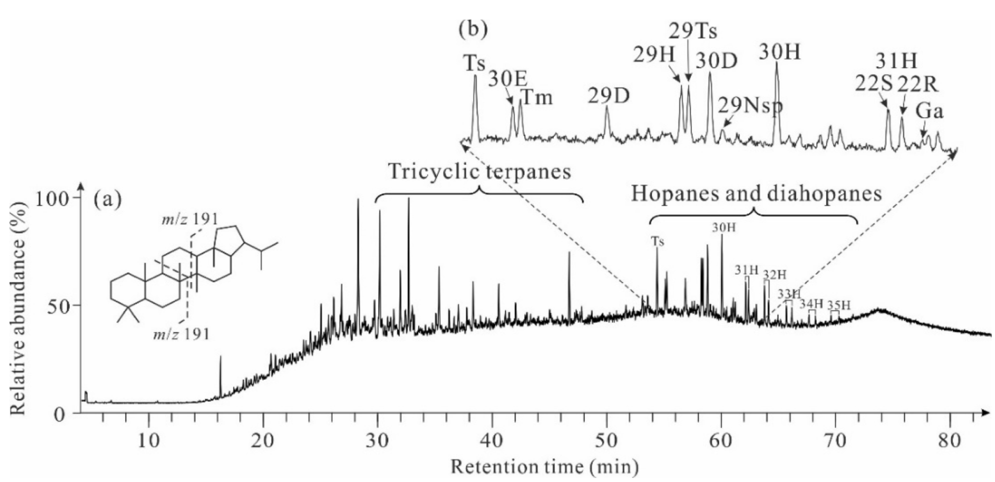


**Fig. 7.** Representative $m/z$ 191 mass chromatogram showing the distribution of regular tricyclic terpanes, regular hopanes and diahopanes in the saturated hydrocarbon of black shale from the Xiamaling Formation. Notes: Ts = $C_{27}$18α(H)-neohopane; 29Ts = $C_{29}$ 18α(H)-neohopane; 30E = $C_{30}$ early eluting rearranged hopane; Tm = $C_{27}$ 17α(H),21β(H)-hopanes; 29D = $C_{29}$ 17α(H)-diahopane; 30D = $C_{30}$ 17α(H)-diahopane; 29Nsp = $C_{29}$ 28-nor-spergulane; Ga = gammacerane.

gammacerane as trace constituent was only slightly above detection limit (Fig. 7b), and the gammacerane index (Ga/$C_{30}$H) shows extremely low average value at 0.05–0.08 (Table 4).

In addition to regular hopanes, four types of rearranged hopanes were simultaneously detected by GC–MS–MS, including the high concentrations of 18α(H)-neohopanes (Ts series), early eluting rearranged hopanes (E series) and 17α(H)-diahopane (D series), and relative low concentration of 28-nor-spergulanes (Nsp series) (Fig. 8). Moreover, minor to moderate concentration of A-ring methylated hopane ($C_{31}$ 2α-methylhopane) was detected (Fig. 8a). The 2α-methylhopane index (Summons et al., 1999) are in the values range of 2.9–3.8 % (Table 4).

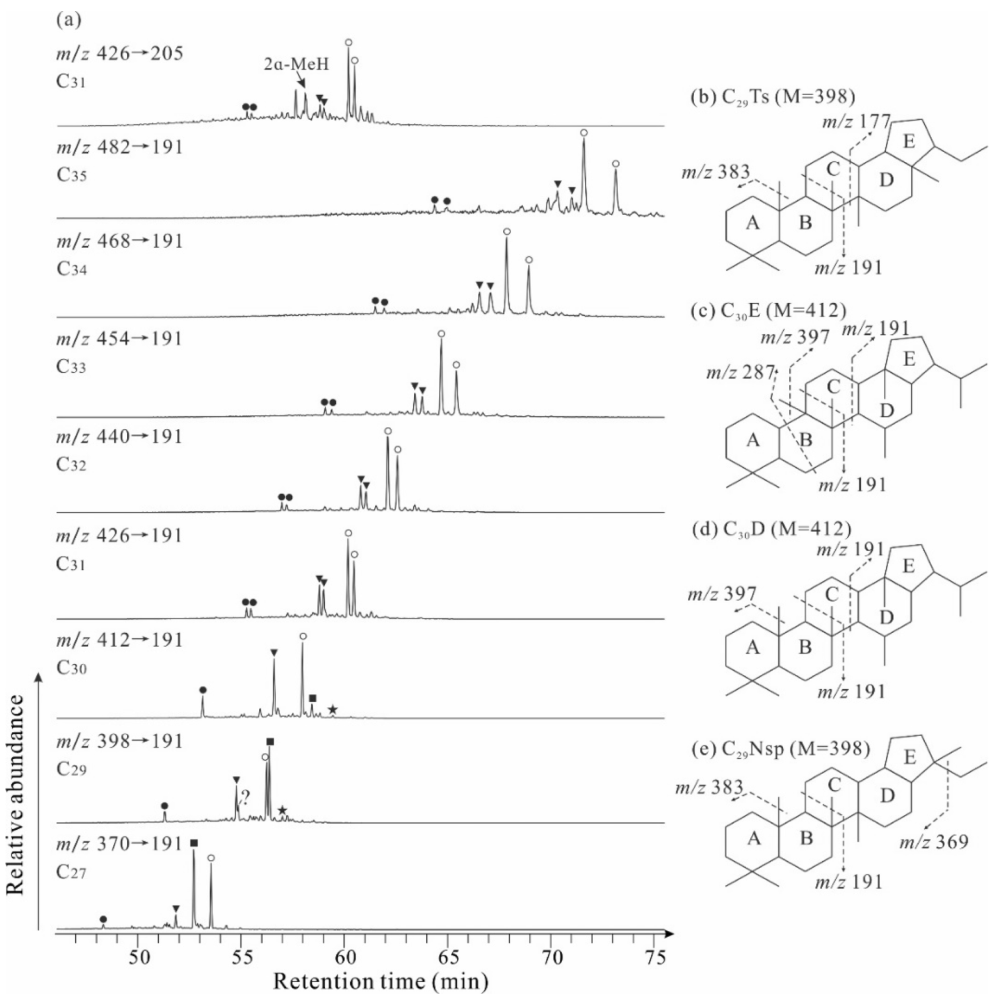


**Fig. 8.** Parent-ion analysis of $m/z$ 191 and $m/z$ 205 daughter ions by gas chromatography-mass spectrometry-mass spectrometry (GC–MS–MS) in the saturated hydrocarbons of black shale from the Xiamaling Formation showing the distribution of regular hopanes, methylhopanes and four series of rearranged hopanes (a), and the molecular structures of rearranged hopanes (b-e). Notes: blank circles = 17α(H),21β(H)-hopanes (H series); solid circles = early eluting rearranged hopane (E series); solid triangles = 17α(H)-diahopane (D series); solid squares = 18α(H)-neohopane (Ts series); solid star = 28-nor-spergulane (Nsp series); 2α-MeH = 2α-methylhopane; 3β-MeH = 3β-methyl hopane.

#### 4.3.4. 13α(n-alkyl)-tricyclic terpanes

A series of unusual tricyclic terpanes, referred as 13α(*n*-alkyl)-tricyclic terpanes (αNATT), was observed in the $m/z$ 123 mass chromatogram of saturated hydrocarbons (Fig. 9). The carbon number of the series compounds ranges from $C_{18}$ to $C_{23}$ with $C_{19}$αNATT as the predominant homolog, which is consistent with the former report (Wang and Simoneit, 1995). The relative concentration of the $C_{19}$αNATT is several times greater than of $C_{30}$H, and the value of $C_{19}$αNATT to $C_{30}$H ratio ($C_{19}$αNATT/$C_{30}$H) ranges from 2.95 to 15.17 (Table 4).

The presence and distribution of αNATT series was also analyzed by specific GC–MS–MS, which revealed an extended series up to $C_{33}$αNATT in the Xiamaling Formation sediments (Fig. 10a). As the carbon number increases from $C_{19}$αNATT to $C_{33}$αNATT, the relative content of homologues gradually decreases (Fig. 10a). Furthermore, the occurrence of $C_{22}$ and $C_{27}$ homologs strongly proves that substituent at C-13 position of αNATTs is a long-chain *n*-alkyl substituent rather than an acyclic isoprenoid (Fig. 10b).

#### 4.3.5. Steranes distribution

Steranes are the diagenetic and catagenetic alteration products of sterols, which are derived from membrane component of most eukaryote (Peters et al., 2005). In the selected ion monitoring traces (SIM) of $m/z$ 217 mass chromatogram of the saturated hydrocarbon of black shale from the Xiamaling Formation, the steroid compounds including $C_{27}$-$C_{29}$ regular steranes, $C_{27}$-$C_{29}$ diasteranes, $C_{30}$ 4-methyl steranes and $C_{21}$-$C_{22}$ short-chain steranes were absent in their habitual

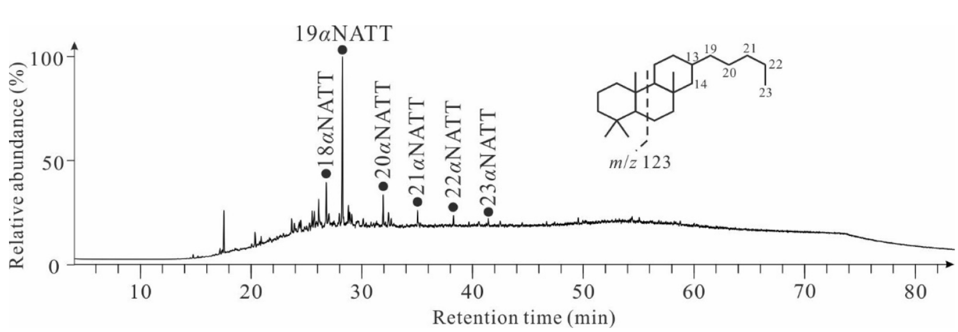


**Fig. 9.** Representative $m/z$ 123 mass chromatogram showing the distribution of $C_{18}$–$C_{23}$ αNATT in the saturated hydrocarbon of black shale from the Xiamaling Formation.

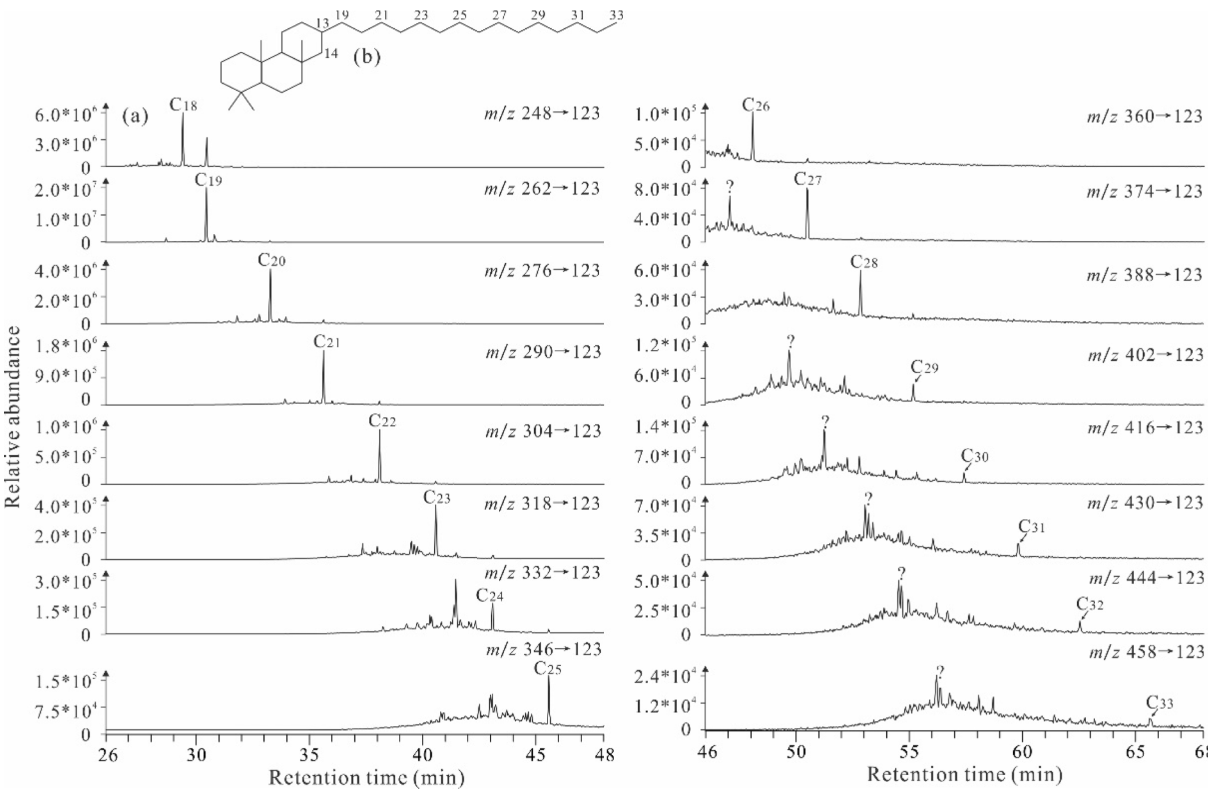

**Fig. 10.** Parent-ion analysis of $m/z$ 191 daughter ions by gas chromatography-mass spectrometry-mass spectrometry (GC–MS–MS) in the saturated hydrocarbon fraction of the Xiamaling Formation sediment extracts, showing the distribution of $C_{18}$–$C_{33}$ 13α($n$-alkyl)-tricyclic terpanes.

retention time range (Fig. 11), which is the same as given in the Touirist Formation sediments (Blumenberg et al., 2012) and the Barney Creek Formation sediments (Brocks et al., 2005). As shown in Fig. 11a, only an apparent hump of baseline was observed in the habitual elution range of steranes, which is composed of unresolved complex mixtures (UCM). In the partially enlarged view of Fig. 11a, only trace amounts of unidentified compounds (marked with "?" in Fig. 11b) can be obviously observed on the hump, which is same as the results of previous study on the Touirist Formation sediments (Blumenberg et al., 2012). Therefore, we could confirm that these unidentified compounds are not contamination derived from exogenous hydrocarbons. Moreover, although we cannot yet accurately identify their molecular structures because of the low contents, the possibility as saturated steroids can be preliminarily excluded based on the retention times of these unidentified compounds and their distribution pattern feature.

### 4.4. Aromatic hydrocarbons

#### 4.4.1. Total ion chromatogram of aromatic hydrocarbons

Aromatic hydrocarbons in shale samples are mainly composed of relatively high abundance of phenanthrene, methyl phenanthrenes, dimethyl phenanthrenes and trimethyl phenanthrenes (Fig. 12), which were generally used to establish indicators for maturity evaluation (Radke et al., 1982a; Radke et al., 1984; Kvalheim et al., 1987). In addition, the samples have the characteristics of very low concentration of trimethyl naphthalenes and tetramethyl napthalenes, and absence of naphthalene, methyl naphthalene and dimethyl naphthalene (Fig. 12). Except for obvious distribution of phenanthrene, alkylphenanthrene,

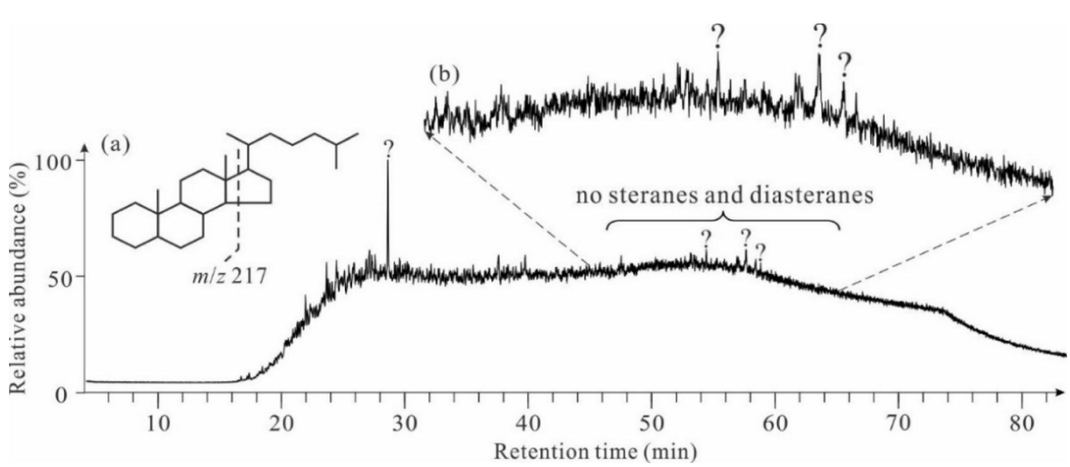


**Fig. 11.** Representative $m/z$ 217 mass chromatogram showing the distribution of regular steranes, diasteranes and short-chain steranes in the saturated hydrocarbon of black shale from the Xiamaling Formation.

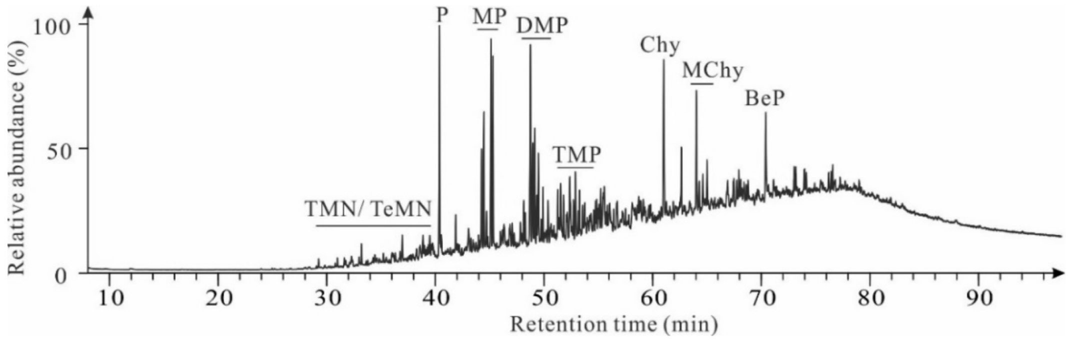


**Fig. 12.** Representative total ion chromatogram of the aromatic fraction of black shale from the Xiamaling Formation. TMN: trimethyl naphthalenes; TeMN: tetramethyl napthalenes; P: phenanthrene; MP: methyl phenanthrenes; DMP: dimethyl phenanthrenes; TMP: trimethyl phenanthrenes; Chy: chrysene; MChy: methyl chrysene; BeP: Benzo[*e*]pyrene.

chrysene, methyl chrysene and Benzo[*e*]pyrene in polycyclic aromatic hydrocarbons (Fig. 12), no other higher molecular weight compounds were detected.

#### 4.4.2. *Aromatic steroids*

Aromatic steroids generally include $C_{26}$-$C_{28}$ triaromatic steroids (*m/z* 231) and $C_{27}$-$C_{29}$ methyl-triaromatic steroids (*m/z* 245). Most Phanerozoic geological samples have obvious distribution of aromatic steroids, which are always used to oil to oil/source rock correlation analyses (Zhang and Huang, 2005; Xiao et al., 2019a). As shown in Fig. 13, neither $C_{26}$-$C_{28}$ triaromatic nor $C_{27}$-$C_{29}$ methyl-triaromatic steroids can be clearly identified, and only an observable hump of baseline substantially develops (Fig. 13). Moreover, abundant trimethyl alkylbenzenes were detected in the *m/z* 134 mass chromatogram, but the isorenieratane and its derivatives (e.g. 2,3,4- and 2,3,6-trimethyl aryl isoprenoids) were absent or in very low concentration in our samples (Fig. 14), which is similar to the 1.38 Ga Velkerri Formation in McArthur Basin (Jarrett et al., 2019).

## 5. Discussion

### 5.1. *Thermal maturity*

#### 5.1.1. *Aromatic hydrocarbon parameters*

In the total ion chromatogram of aromatic hydrocarbons, phenanthrene and its methyl substituted compounds show prominent concentrations (Fig. 12). As the effective thermal maturity-dependent aromatic hydrocarbon ratios, methyl phenanthrene ratio (MPR), methyl phenanthrene indices (MPI-1), (3-+2-MP)/SMPs (F1), 2-MP/SMPs (F2) ratios were extensively used in the maturity evaluation of source rocks and oils (Radke et al., 1982a; Radke et al., 1982b; Kvalheim et al., 1987; Bao et al., 1992; Brocks et al., 2003c). In these samples, the values of MPR and MPI-1 are in the range of 0.49–0.78 and 0.22–0.47, respectively (Table 5). The equivalent vitrinite reflectance of MPR ($R_{MPR}$, %) (Radke et al., 1984) and MPI-1 ($R_c$, %) (Radke and Welte, 1983) varies from 0.64 % to 0.83 % and 0.53–0.68 %, respectively (Table 5). These maturity related-parameters indicate that the organic matter is still in the early stage of hydrocarbon generation window. Furthermore, the

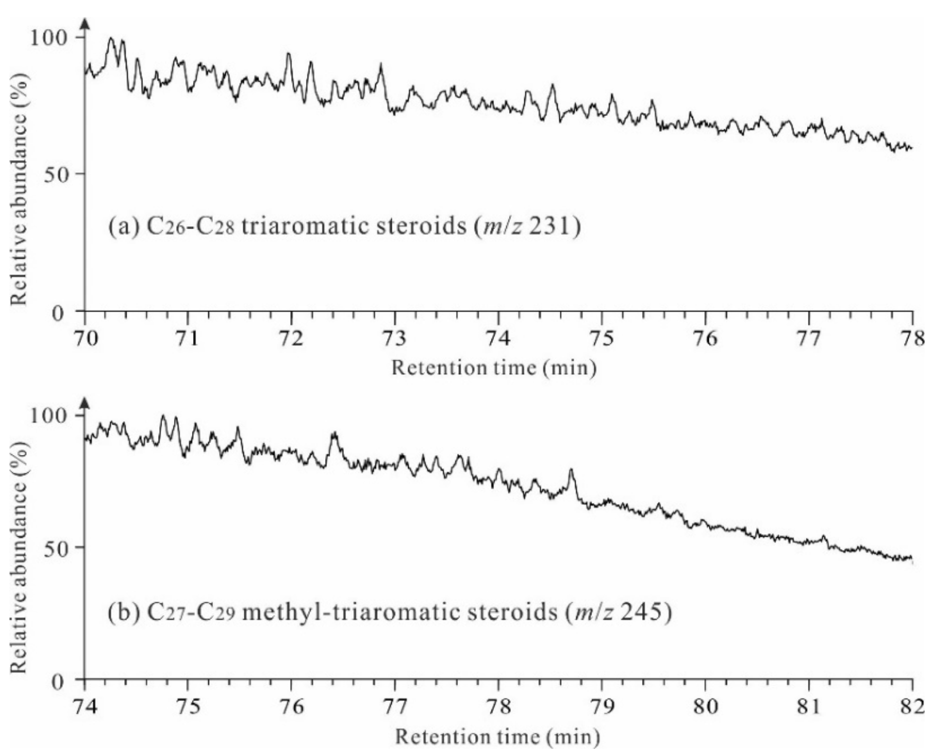


**Fig. 13.** Representative mass chromatograms showing the distribution of $C_{26}$-$C_{28}$ triaromatic steroids (a) and $C_{27}$-$C_{29}$ methyl-triaromatic steroids (b) in the aromatic fraction of black shale from the Xiamaling Formation.

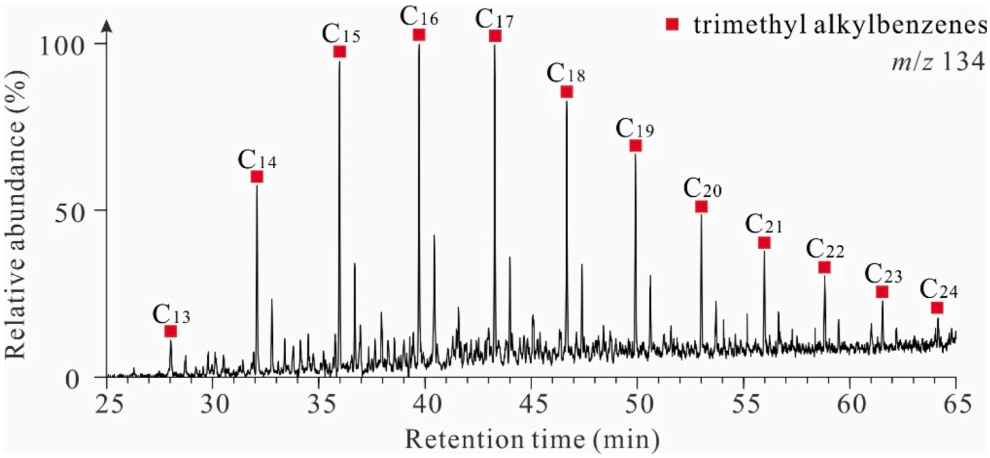


**Fig. 14.** Partial *m/z* 134 mass chromatogram in the aromatic fraction of black shale from the Xiamaling Formation.

**Table 5**
Maturity indicators of aromatic hydrocarbons and calculated vitrinite reflectance of black shales from the Xiamaling Formation in the North China Craton.

| Sample | Formation | MPR | $R_{MPR}$ (%) | MPI-1 | $R_c$ (%) | F1 | F2 | $R_b$ (%) | $R_o$ (%) |
|---|---|---|---|---|---|---|---|---|---|
| XHY_1 | Xiamaling | 0.56 | 0.69 | 0.30 | 0.58 | 0.18 | 0.11 | 0.46 | 0.68 |
| XHY_2 | Xiamaling | 0.49 | 0.64 | 0.35 | 0.61 | 0.20 | 0.11 | 0.46 | 0.68 |
| XHY_3 | Xiamaling | 0.57 | 0.70 | 0.37 | 0.62 | 0.21 | 0.12 | 0.48 | 0.70 |
| XHY_4 | Xiamaling | 0.55 | 0.68 | 0.39 | 0.64 | 0.23 | 0.13 | 0.49 | 0.70 |
| XHY_5 | Xiamaling | 0.70 | 0.79 | 0.42 | 0.65 | 0.31 | 0.19 | – | – |
| XHY_6 | Xiamaling | 0.75 | 0.82 | 0.43 | 0.66 | 0.34 | 0.16 | – | – |
| XHY_7 | Xiamaling | 0.73 | 0.80 | 0.47 | 0.68 | 0.36 | 0.21 | – | – |
| XHY_8 | Xiamaling | 0.74 | 0.81 | 0.22 | 0.53 | 0.37 | 0.28 | – | – |
| XHY_9 | Xiamaling | 0.78 | 0.83 | 0.45 | 0.67 | 0.37 | 0.24 | – | – |

Notes: MPR = 2-/1-MP; $R_{MPR}$ = (0.99*log10 MPR) + 0.94; MPI-1 = 1.5*(3-+2-MP)/(P + 9-+1-MP); $R_c$ = 0.6*MPI + 0.4; F1 = (3-+2-MP)/SMPs; F2 = 2-MP/SMPs; $R_o$ = 0.618*$R_b$ + 0.4; '-' = no data.

cross-plot of F1 vs F2 proposed by Bao et al. (1992) is usually used to evaluate thermal maturity levels. All samples contain low values of F1 and F2 ratios, less than 0.37 and 0.28 respectively (Table 5), completely falling into the region of low maturity (Fig. 15) (Bao et al., 1992).

### 5.1.2. Bitumen reflectance and pyrolysis parameter

In addition to the maturity parameters related to phenanthrene series compounds, protobitumen reflectance ($R_b$) with the value rang of 0.46–0.49 % (Table 5), equivalent vitrinite reflectance of $R_b$ ($R_o$) with the averaged values of 0.69 % (Table 5), Rock-eval pyrolysis parameter (Tmax) with the averaged values of ~437 °C (Table 1) and $C_{31}$-$C_{32}$ homohopane isomerization parameters with the value rang of 0.55–0.58 (Table 4) were comprehensively analyzed to determine the thermal evolution stage. All samples presented internally consistent molecular data and were in the early stage of oil generation window. Because the 18α(H)-neohopane was considered to be controlled by clay mineral-catalyzed diagenetic reactions, and derived from multiple sources (Farrimond and Telnæs, 1996; Xiao et al., 2019b), especially in this study, all samples have abnormally abundant four rearranged hopane series (e.g. neohopane series), thus the thermal maturity parameters related to rearranged hopanes, such as Ts/(Ts + Tm) ratio, are invalid.

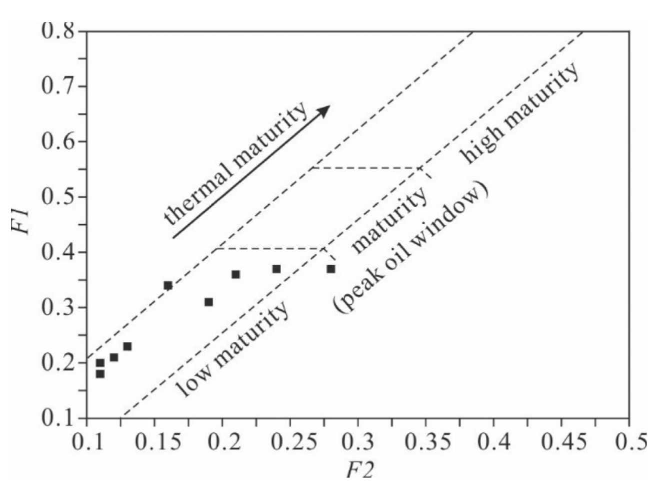


**Fig. 15.** Plate of maturity indicators related to methyl phenanthrene. Notes: F1 = (3-+2-MP)/SMPs; F2 = 2-MP/SMPs; SMPs = 3-MP + 2-MP + 9-MP + 1-MP.

## 5.2. Biomarker syngeneity

Lipid biomarkers can reveal significant signals for the evolution of microbial ecosystem and sedimentary environments in Earth's history, but the syngeneity of organic matter is a prerequisite (Rasmussen et al., 2008; Ai et al., 2020). Generally, the vast majority of the Precambrian sediments have entered a stage of high- to over-maturity thermal evolution, containing extremely low content of solvent extracted hydrocarbons. Consequently, the indigenous signals are easily overprinted by any contaminants from external environment, including modern contamination during the processes of drilling, sampling, transportation, preservation and experimental analysis, and geological contamination of migrating hydrocarbons generated from adjacent younger source rocks (Brocks, 2011; Ai et al., 2020). Therefore, the prerequisites of using biomarkers to explore the paleo-sedimentary environment, paleo-ecosystem, and life evolution of the early earth is that the extracted hydrocarbon is indigenous and syngenetic. Recently, various effective methods for extracting indigenous hydrocarbons from Precambrian sediments to avoid later contamination have been well established, including slice experiments (Sherman et al., 2007; Brocks, 2011; French et al., 2015) and micro-ablation for the bitumen phase (Jarrett et al., 2013), and catalytic hydropyrolysis (HyPy) for parallel analysis of the kerogen-bound pool (Love et al., 1995; Love et al., 2005; Love et al., 2008).

Significantly, these black shales in this study have not only a high abundances of soluble organic matter (Table 1 and Fig. 3a), but also a low degree of thermal maturity (Tables 1 and 5, and Fig. 3b), which was never heated to above 90 °C, thus well-preserving organic biomarkers (Zhang et al., 2015). The black shale samples are unique and completely different from the common Precambrian sediments, so they are not easily contaminated by external hydrocarbons. In addition, the direct evidence for syngeneity of the lipid biomarkers in the study were showed as following. First, all samples contain typical molecular characteristics of Proterozoic bitumen, such as an obviously large UCM and abundant branched alkanes (Fig. 5) (Pawlowska et al., 2013). Second, steranes (e.g. regular steranes, short-chained steranes and diasteranes) and aromatic steroids were absent or below detection limit in the extracted hydrocarbons (Figs. 11 and 13), which further strengthened the view of no contamination from the Phanerozoic hydrocarbons. Furthermore, all the maturity parameters including Tmax, MPI-1, MPDF, MPR, and bitumen reflectance ($R_b$, %) reflect the same degree of thermal evolution, still in low maturity stage.

From the above, these signals offer convincing evidence for the syngeneity and indigeneity of hydrocarbon biomarkers from the Xiamaling Formation black shales.

### 5.3. *Microbial reworking*

#### 5.3.1. *Unresolved complex mixture (UCM)*

Compared with Phanerozoic bitumen, the Proterozoic bitumen always contains a notably unresolved complex mixture (UCM) (Pawlowska et al., 2013). The UCM is thought to consist of thousands of unidentified branched and cyclic hydrocarbons. When there is obvious UCM in the gas chromatograms of Phanerozoic oils, in the instances it is generally suggested that it was caused by microbial degradation after the crude oil was expelled from the parent rock into the shallow reservoirs (Peters et al., 2005). However, the visible UCM was also widely found in most Proterozoic bitumen (Summons et al., 1988b; Kelly et al., 2011; Pawlowska et al., 2013; Luo et al., 2015; Luo et al., 2016; Bhattacharya et al., 2017) even if it is still preserved in the parent rock. The widespread hump of UCM, as one of typical characteristics of Proterozoic bitumen may be attributed to microbial reworking of primary lipid organic matter by bacterial microbial communities either on photosynthetic benthic mats (Pawlowska et al., 2013) or in the sedimentary water column (Logan et al., 1995).

In this light, the ubiquitous UCM hump in Proterozoic bitumen could be excluded as the product of late-stage microbial degradation in shallow reservoirs, but regarded as the severely biodegraded product from the plankton and upper microbial mat during the early stage. This scenario reveal that Proterozoic organic matter has fundamental difference in taphonomy and preservation processes from Phanerozoic organic matter, which is caused by the pervasive presence of Proterozoic “mat-seal effect” (Pawlowska et al., 2013), and also so-called biases of lipids taphonomy.

#### 5.3.2. *Abundant monomethyl alkanes (MMAs)*

The relative abundance of monomethyl alkanes (MMAs) in Proterozoic bitumen is also conspicuously higher than that of the Phanerozoic counterparts. Since the MMAs isomers are radically different from all known biological sources, the early recognition is that the widespread MMAs fossils are likely to be produced by the cleavage and/or rearrangement reactions of functionalized precursors (Kissin, 1987). However, Shiea et al. (1990) found abundant MMAs in modern hot spring microbial mats, indicating that MMAs may be produced from direct biogenic contributions, such as cyanobacteria, eubacteria, and/or heterotrophic bacteria (Shiea et al., 1990; Kenig, 2000). In addition, Audino et al. (2001) detected four homologous series of MMAs in the soluble hydrocarbons and the catalytic hydropyrolysis products of Permian torbanites, and observed the that MMAs was markedly enriched in $^{13}C$ compared with normal alkanes (Audino et al., 2001), which was consistent with the previous report (Kenig et al., 1994). One explanation for the scenario was that the heterotrophic bacteria preferentially utilize isotopically heavy carbohydrate and protein fractions, rather than depleted-$^{13}C$ lipid fraction within the same organism (Audino et al., 2001). Therefore, the presence of unusual distribution of isotopically heavy MMAs was possibly indicative of severe heterotrophic reworking of the algal biomass within microbial mats (Pawlowska et al., 2013; Jarrett et al., 2019).

#### 5.3.3. *Distribution of steranes*

The dearth of saturated and aromatic steroids (Figs. 11 and 13) in these sediments is a largely faithful biomarker representation of minimal contribution of eukaryotes to the ancient marine ecosystems during the deposition period of Xiamaling Formation in the Xiahuayuan area (Anbar and Knoll, 2002; Blumenberg et al., 2012; Luo et al., 2015; Jarrett et al., 2019; Nguyen et al., 2019). However, the ancient lipid biomarkers, like microfossils, may also be affected by many biases of the taphonomy pathways, resulting in the loss of the biological signals (Logan et al., 1995; Butterfield, 2003; Pawlowska et al., 2013).

Recently, Pawlowska et al. (2013) proposed a new explanation for the paucity of eukaryotic steranes in the mid-Proterozoic sediments, a hypothetical mechanism termed the “mat-seal effect”. This explanation suggested that the severe heterotrophic microbial reworking of planktonic eukaryotic communities by the widespread benthic microbial mats in the shallow water environments can also results in lack of steroids (Pawlowska et al., 2013). Based on the analysis of a modern calcifying microbial mats (~1500 years) from the hypersaline lakes on the island of Kiritimati, it is found that the total sterol concentration in the deep layers was significantly reduced by 98 % (Shen et al., 2020) and the values of hopane/sterane ratio exceed 20 (Blumenberg et al., 2015). In contrast, Lee et al. (2019, 2021) reported that significant amounts of steranes and hopanes were simultaneously preserved in the hypersaline microbial mats and underlying sediments at Guerrero Negro, which argued against the tendency of “mat-seal effect” to preferentially destroy steroids (Lee et al., 2019, 2021). Taken together, the extent of microbial reworking for primary eukaryotic sterols in benthic microbial mats remains controversial, which may be controlled by multiple biotic or abiotic factors.

However, Miao et al. (2021) recently reported a moderate diversity of eukaryotic microfossil in the Xiamaling Formation shales from the Tielingzi section in NCC, which may suggest that eukaryotic algae have been locally evolved during the depositional period of the Xiamaling Formation in NCC (Miao et al., 2021). Combining the undetected steroids and the local findings of eukaryotic fossils, we speculated that the absence of steranes in the Xiamaling Formation from the Xiahuayuan section may be results of the limited contribution of eukaryotic algae and/or microbial reworking duo to “mat-seal effect” (Luo et al., 2015).

### 5.4. *Paleoenvironments*

The Xiamaling Formation black shales in NCC were deposited in the mid-Proterozoic at about ~1.40 Ga, which have high amounts of organic matter and low thermal maturity. The micro-ripples observed in the samples generally suggested shallow condition during deposition of benthic mats (Fig. 4). The biomarker compositions of soluble hydrocarbons from the Xiamaling Formation have the characteristics of moderate values of Pr/Ph ratio, low values of gammacerane index (Ga/$C_{30}$H), homohopane index (HHI = $C_{35}H/C_{31-35}H$) (Tables 3-4), low contents of DBT series (Fig. 12) and high abundance of rearranged hopanes (Fig. 8), as well as absence of aryl isoprenoids and their chemical relicts (e.g. 2,3,6-trimethyl aryl isoprenoids) (Fig. 14), which indicates shallow, low salinity, and suboxic water conditions during deposition of the Xiamaling Formation. Moreover, it further argued against the pervasively euxinic (sulphidic) bottom water in mid-Proterozoic ocean (Canfield, 1998; Brocks et al., 2005; Canfield, 2005).

### 5.4.1. Pristane/phytane ratio (Pr/Ph)

In 1969, Brooks et al. proposed that Pr/Ph ratio can reflect the degree of oxidation during early diagenesis of chlorophyll (Brooks et al., 1969). Generally, Pr/Ph ratio of our samples with the value range of 0.71–0.91 neither suggests extremely reductive ($\ll$1.0) nor oxidative ($\gg$1.0) conditions (Table 3) (Peters et al., 2005). With properly considering the restricted utility of Pr/Ph ratio as an indicator of oxygen levels (Goossens et al., 1984; ten Haven et al., 1987), and our limited knowledge of the oxicity of sedimentary environment, Pr/Ph values tend to favor suboxic to anoxic conditions (Table 3).

### 5.4.2. Rearranged hopanes

High abundance and widespread existence of rearranged hopanes in the Xiamaling Formation black shales further supports the suboxic to anoxic depositional conditions (Fig. 8). Generally, rearranged hopanes exhibit relatively strong resistance to biodegradation and high thermal stability (Kolaczkowska et al., 1990; Moldowan et al., 1991; Xiao et al., 2019b). In Proterozoic bitumen, various type of rearranged hopanes have been occasionally reported (Summons et al., 1988a; Dutkiewicz et al., 2004; Wang et al., 2018; Xiao et al., 2021a). Although the origin of the rearranged hopanes is still controversial, thermal maturity was directly excluded as the main controlling factor for the occurrence of abundant rearranged hopanes in the study, as all samples exhibit low Rc values in the range of 0.53–0.68 % (Table 5). Likewise, biodegradation can also be excluded because biodegradation is always used to characterize the secondary changes of crude oil, and all samples have no trace of biodegradation, such as the obvious loss of normal alkanes (Fig. 5) and the distribution of 25-norhopane (Fig. 7). The latest research revealed that the atmospheric oxygen levels during the deposition period of the Xiamaling Formation can reach > 4 % of current oxygen level (Zhang et al., 2016). Wang et al. (2018) further proposed that the bottom waters is oxic during the deposition of Member 3 of the Xiamaling Formation, and the relative higher dissolved oxygen led to the transformation of hopane precursors into rearranged hopanes in the early diagenetic stage. Therefore, we speculate that the presence of abundant rearranged hopanes in the Xiamaling Formation black shales likely reflect shallow and suboxic depositional environment, which is conducive to the rearrangement reactions (Moldowan et al., 1991; Wang et al., 2018; Jarrett et al., 2019), or the prosperity of some specific bacterial communities (their potential precursors) (Xiao et al., 2021a).

### 5.4.3. Aryl isoprenoids and dibenzothiophenes (DBT)

Dibenzothiophenes (DBTs) is one of the most important sulfur-containing compounds in bitumen. It has no definite biological precursor but was considered to be mainly formed by a catalytic reaction between elemental sulfur/sulfur radicals and organic material in the early stage of diagenesis (Douglas and B.J., 1965; Hughes et al., 1995; Asif et al., 2009; Li et al., 2013). The 2,3,4- and 2,3,6-trimethyl aryl isoprenoids were diagenetic break-down products of $C_{40}$ carotenoids producing from green/purple sulfur bacteria (Summons and Powell, 1986; Brocks and Schaeffer, 2008). Recently, Brocks et al. (2005) detected high amounts of aryl isoprenoids biomarkers in the Barney Creek Formation black shales (~1.64 Ga) from the McArthur Basin, revealing sulphidic and permanently stratified deep waters (Brocks et al., 2005). However, the absence of aryl isoprenoids and trace amounts of DBTs (Figs. 12 and 14), together with the moderate Pr/Ph values, abundant rearranged hopanes and low gammacerane index values (Tables 3-4) further suggest a suboxic to anoxic water condition during the depositional period of the Xiamaling Formation black shales. The absence or very low abundance of aryl isoprenoids in the 1.3–1.4 Ga Velkerri Formation shales of the McArthur Basin also supported the suboxic to anoxic conditions rather than euxinic in the photic zone (Jarrett et al., 2019; Nguyen et al., 2019).

### 5.4.4. Redox-sensitive trace elements

In addition to the evidence from biogeochemical signatures, the redox-sensitive trace elements also supported the same conclusion. As shown in Table 6, the black shales of Xiamaling Formation contain very low content of trace element amounts (Zn, V, U) and low values of V/(V + Ni) ratio (0.47–0.65), which indicates an suboxic to anoxic conditions and weakly stratified water column (Hatch and Leventhal, 1992). Moreover, high Mo concentrations (tens to hundreds, ppm) are diagnostic of deposition under euxinic conditions (Lyons et al., 2009). Significantly low Mo concentration with the value range of 6.19 ppm to 7.28 ppm (Table 6) further reflects non-euxinic conditions during deposition period of the Xiamaling Formation in NCC. It is extremely lower than the Cariaco Basin sediments in the Venezuela (up to 184 ppm) (Lyons et al., 2003) and the 1.84 Ga Rove Formation black shales (up to 50 ppm) (Scott et al., 2008) which were deposited in euxinic (sulphidic) bottom water condition. Generally, in anoxic and containing $H_2S$ water column, the sulfophilic elements like Fe, Cu and Zn are often easy to form sulfide precipitation, but no pyrite ($FeS_2$) was observed in hand specimens or microscopic sections (Fig. 4).

The suboxic to anoxic conditions during the deposition period of the Xiamaling Formation further argues against the widely and perhaps even globally euxinic (sulphidic) deep-ocean water conditions persisted from late Paleoproterozoic (~1.80 Ga) to Neoproterozoic Oxidation Event (~0.80 Ga) (Canfield, 1998; Brocks et al., 2005). The absence of euxinic conditions above the benthic microbial mat of the Xiamaling Formation may reflect the shallow water environment and the possibility for increased oxygen diffusion from the atmosphere to water or the effects of occasional storm (Blumenberg et al., 2012), which was strongly supported by the relatively high atmospheric oxygen levels (>4%) (Zhang et al., 2016). This result is also consistent with the former report of Luo et al. (2015) that all facies members of the Xiamaling Formation appear to be anoxic but not euxinic (sulphidic) (Luo et al., 2015). Moreover, previous results of the redox-sensitive metal concentrations and lipid biomarkers in the similarly aged shales from the 1.3–1.4 Ga Velkerri Formation (Jarrett et al., 2019; Nguyen et al., 2019) and the 1.1 Ga Touirist Formation (Blumenberg et al., 2012) also proposed the suboxic to anoxic conditions prevailing in shallow water during mid-Proterozoic.

## 5.5. Primitive organismic community

### 5.5.1. Prokaryotes

In modern sedimentary organic matters, *n*-alkanes can be derived from higher plant waxes (mainly producing high carbon number series) (Hedberg, 1968), polymethylenic biopolymers from eukaryotic algae (Tegelaar et al., 1989), and phospholipids in bacterial or eukaryotic cell membranes. The higher plant source to *n*-alkanes can be decidedly excluded for the pre-Silurian samples, and the contribution of polymethylenic biopolymers in the mid-Proterozoic is negligible (Brocks et al., 2003b). Therefore, the predominance of low-molecular-weight *n*-alkanes (Fig. 4) indicates that the organic matter inputs mainly consists of bacteria, cyanobacteria and/or planktonic algae. Of special interest is that the predominance of high-molecular-weight *n*-alkanes have also been found in other Mesoproterozoic and even much older rocks, such as Gaoyuzhuang Formation (Li et al., 2001, 2003; Cui, 2011; Wang and

**Table 6**
Zn, V, U and Mo contents, and values of V/(V + Ni) ratio for three black shale samples from the Xiamaling Formation.

| Sample | Formation | Zn/ppm | V/ppm | U/ppm | Mo/ppm | V/(V + Ni) |
|---|---|---|---|---|---|---|
| XHY_1 | Xiamaling | 64.0 | 52.6 | 2.46 | 6.79 | 0.48 |
| XHY_2 | Xiamaling | 67.2 | 53.5 | 2.47 | 7.28 | 0.47 |
| XHY_4 | Xiamaling | 108.0 | 108.0 | 2.50 | 6.19 | 0.65 |

Han, 2011). The scenario of uncommon *n*-alkanes distribution pattern in mid-Proterozoic bitumen was explained as the contribution of multiple inputs from complicated biological assemblages (Li et al., 2001, 2003). Considering that *n*-alkanes and *n*-alkylcyclohexanes exhibit extremely consistent distribution pattern, including their carbon number range and major peaks, it is proposed that they have similar biological sources, mainly from bacteria and/or cyanobacteria.

13β(H),14α(H)-tricyclic terpanes (TTs) are ubiquitous in various geological samples from Proterozoic to Phanerozoic and viewed as 'orphan biomarkers' due to the lack of clear biologic precursors (Rohmer et al., 1992; Ourisson, 1994). The TTs have been widely considered (but not proven) to be a suitable stabilizing constituent of membranes of prokaryotic microorganisms (Aquino Neto et al., 1982) or derived from the now-extinct *Tasmanites* (Simoneit et al., 1990; Greenwood et al., 2000; Dutta et al., 2006). However, the short-chain tricyclic terpenes ($C_{19}$-$C_{20}$TT) are frequently enriched in coal-measure samples and usually indicates the contribution of higher plant (Ekweozor, 1984), such as the dammarenes from diptrocarpol and methylisoanticopalate from manool (Aquino Neto et al., 1982). Although TTs might have multiple sources, the conspicuous predominance of $C_{19}$-$C_{20}$TTs in the sterane-free samples suggested that prokaryotic microorganisms may be the main source of $C_{19}$-$C_{20}$TTs, unlike previous studies on the Phanerozoic sediments (Ekweozor, 1984; Greenwood et al., 2000; Xiao et al., 2019c). Except for regular tricyclic terpanes, 13*α*(*n*-alkyl)-tricyclic terpane series was distinctly detected in the Xiamaling Formation, which was considered to be derived from a limited number of bacteria and/or cyanobacteria (Wang and Simoneit, 1995). Moreover, its distribution range in whole geological period is very limited, indicating that it may be derived from several specific bacteria living in limited conditions (Xiao et al., 2021b). For example, it is not prosperous during the depositional period of the Gaoyuzhuang Formation (Sun and Wang, 2016), and disappeared in the Phanerozoic.

Importantly, the vast majority of biological contributions are probably composed of bacteria and cyanobacteria in the Xiamaling Formation black shales, as supported by the abundant hopane series including $C_{27}$-$C_{35}$ regular hopanes, rearranged hopanes and 2α-methylhopanes. Generally, 2α-methylhopane index (2-MHI) has been frequently used to characterize the contributions of cyanobacteria (Summons et al., 1999). However, further studies have shown that 2α-methylhopane is not the unique biomarker for cyanobacteria, and a large number of modern marine cyanobacteria are free of 2-methylhopane precursors (Talbot et al., 2008). Therefore, relative low values of 2α-methylhopane index in the range of 2.9–3.8 % (Table 4) cannot exclude considerable contributions of cyanobacteria.

In summary, the abundant *n*-alkanes, *n*-alkylcyclohexanes, tricyclic terpanes and hopanoids in the black shales of the Xiamaling Formation therefore support the scenario of predominant contribution of bacteria/cyanobacteria.

#### 5.5.2. *Eukaryotes*

Generally, Proterozoic biomarker assemblages are characterized by conspicuously low concentrations or absence of eukaryotic steranes. The paucity of steranes in the mid-Mesoproterozoic was often interpreted as limited ecological significance of eukaryotes (Anbar and Knoll, 2002; Blumenberg et al., 2012; Luo et al., 2015; Jarrett et al., 2019; Nguyen et al., 2019). Accordingly, the saturated steroids (e.g. regular steranes, diasteranes and short-chained steranes) (Fig. 11) and aromatic steroids (e.g. triaromatic and methyl-triaromatic steroids) (Fig. 13) were absent or under detection limit in the black shales of the Xiamaling Formation, suggesting minor significance of eukaryotic algae to primitive ecosystem.

Although the microbial fossil is the most effective method for assessing the existence of eukaryotes and a moderate diversity of eukaryotic microfossil have been locally found in the Xiamaling Formation shales from the Tielingzi section in NCC (Miao et al., 2021), discernible microfossils represent only a small fraction of the total amount of primitive organic matter (Nguyen et al., 2019). Therefore, it is difficult to convince that eukaryotes make significant contributions to primitive organic matter without detectable diagnostic biomarkers in the Xiamaling Formation shales. While some hypoxia-adapted eukaryotes lack sterol structures in their cell membranes, only a few anaerobic protists are likely to be part of the primitive community structure (Takishita et al., 2017). The probable mass of microbial reworked and sterol-free eukaryotes is extremely limited relative to prevalence prokaryotic bacteria or cyanobacteria. Therefore, a fundamental conclusion of this study is that eukaryotic algae have little ecological contribution to primitive biomass to the mid-Proterozoic ocean in NCC, indicating that eukaryotes were not the dominant role of primary producers.

## 6. Conclusions

The 1.40 billion-year-old (Ga) Xiamaling Formation (XML) black shale in the NCC contains abundant low-maturity soluble hydrocarbons, which are identified as syngenetic from molecular markers and thermal maturity indicators. A persistently shallow, low salinity, suboxic to anoxic and non-sulfidic paleo-ocean environment was reconstructed by molecular fossils and redox-sensitive trace elements, which argues against pervasive euxinic condition in the mid-Proterozoic ocean. The enrichment of *n*-alkanes, *n*-alkylcyclohexanes, tricyclic terpanes and hopane series demonstrates that bacteria and cyanobacteria are the most important members of the primary biological assemblage in the mid-Proterozoic ocean. The absence of saturated and aromatic steroids suggested that eukaryotic algae have little ecological contribution to primitive biomass and/or are the result of heterotrophic reworking from benthic microbial mats.

## CRediT authorship contribution statement

**Hong Xiao:** Writing – original draft, Writing – review & editing. **Meijun Li:** Conceptualization, Funding acquisition. **Tieguan Wang:** Supervision, Resources. **Bing You:** Writing – review & editing. **Xiaolin Lu:** Data curation. **Xin Wang:** Methodology.

## Declaration of Competing Interest

The authors declare that they have no known competing financial interests or personal relationships that could have appeared to influence the work reported in this paper.

## Acknowledgements

The authors would like to thank Dr. Frances Westall (Editor) and anonymous reviewers for the constructive comments and suggestions which significantly improved the quality of the manuscript. This work was supported by the National Key Research and Development Program of China (No. 2017YFC0603102).

## References

Ai, J.Y., George, S.C., Zhong, N.N., 2020. Organic geochemical characteristics of highly mature Late Neoproterozoic black shales from South China: Reappraisal of syngeneity and indigeneity of hydrocarbon biomarkers. Precambrian Res. 336, 105508.
Alpern, B., 1980. Sedimentary organic matter and kerogen. Petrographie du Kerogene. In: Durand, B. (Ed.), Kerogene, Insoluble Organic Matter From Sedimentary Rocks. France, Technip, Paris, pp. 339–384.
Anbar, A.D., Knoll, A.H., 2002. Proterozoic ocean chemistry and evolution: a bioinorganic bridge? Science 297, 1137–1142.
Aquino Neto, F.R., Restle, A., Connan, J., Albrecht, P., Ourisson, G., 1982. Novel tricyclic terpanes (C19, C20) in sediments and petroleums. Tetrahedron Lett. 23, 2027–2030.
Aquino Neto, F.R., Trendel, J.M., Restlé, A., Connan, J., Albrecht, P., 1983. Occurrence and formation of tricyclic terpanes in sediments and petroleums. In: Bjorøy, M., Albrecht, P., Cornford, C., de Groot, K., Eglinton, G., Galimov, E., Leythaeuser, D., Pelet, R., Rullkötter, J., Speers, G. (Eds.), Advances in Organic Geochemistry 1981. Wiley, Chichester, pp. 659–667.

Asif, M., Alexander, R., Fazeelat, T., Pierce, K., 2009. Geosynthesis of dibenzothiophene and alkyl dibenzothiophenes in crude oils and sediments by carbon catalysis. Org. Geochem. 40, 895–901.

Audino, M., Grice, K., Alexander, R., Boreham, C.J., Kagi, R.I., 2001. Unusual distribution of monomethylalkanes in Botryococcus braunii–rich samples: origin and significance. Geochim. Cosmochim. Acta 65, 1995–2006.

Bao, J., Wang, T., Zhou, Y., Yu, F., Wang, J., ZHou, Q., Chen, F., 1992. The Relationship between Methyl Phenanthrene Ratios and the Evolution of Organic Matter. J. Jianghan Petrol. Inst. 14, 8–19 (in Chinese).

Bhattacharya, S., Dutta, S., Summons, R.E., 2017. A distinctive biomarker assemblage in an Infracambrian oil and source rock from western India: Molecular signatures of eukaryotic sterols and prokaryotic carotenoids. Precambrian Res. 290, 101–112.

Blumenberg, M., Thiel, V., Riegel, W., Kah, L.C., Reitner, J., 2012. Biomarkers of black shales formed by microbial mats, Late Mesoproterozoic (1.1Ga) Taoudeni Basin. Mauritania. Precambrian Res. 196–197, 113–127.

Blumenberg, M., Thiel, V., Reitner, J., 2015. Organic matter preservation in the carbonate matrix of a recent microbial mat – Is there a 'mat seal effect'? Org. Geochem. 87, 25–34.

Bobrovskiy, I., Hope, J.M., Ivantsov, A., Nettersheim, B.J., Hallmann, C., Brocks, J.J., 2018a. Ancient steroids establish the Ediacaran fossil Dickinsonia as one of the earliest animals. Science 361, 1246–1249.

Bobrovskiy, I., Hope, J.M., Krasnova, A., Ivantsov, A., Brocks, J.J., 2018b. Molecular fossils from organically preserved Ediacara biota reveal cyanobacterial origin for Beltanelliformis. Nat. Ecol. Evol. 2, 437.

Brocks, J.J., 2011. Millimeter-scale concentration gradients of hydrocarbons in Archean shales: Live-oil escape or fingerprint of contamination? Geochim. Cosmochim. Acta 75, 3196–3213.

Brocks, J.J., Schaeffer, P., 2008. Okenane, a biomarker for purple sulfur bacteria (Chromatiaceae), and other new carotenoid derivatives from the 1640Ma Barney Creek Formation. Geochim. Cosmochim. Acta 72, 1396–1414.

Brocks, J.J., Logan, G.A., Buick, R., Summons, R.E., 1999. Archean molecular fossils and the early rise of eukaryotes. Science 285, 1033–1036.

Brocks, J.J., Buick, R., Logan, G.A., Summons, R.E., 2003a. Composition and syngeneity of molecular fossils from the 2.78 to 2.45 billion-year-old Mount Bruce Supergroup, Pilbara Craton. Western Australia. Geochim. Cosmochim. Acta 67, 4289–4319.

Brocks, J.J., Buick, R., Summons, R.E., Logan, G.A., 2003b. A reconstruction of Archean biological diversity based on molecular fossils from the 2.78 to 2.45 billion-year-old Mount Bruce Supergroup, Hamersley Basin. Western Australia. Geochim. Cosmochim. Acta 67, 4321–4335.

Brocks, J.J., Summons, R.E., Buick, R., Logan, G.A., 2003c. Origin and significance of aromatic hydrocarbons in giant iron ore deposits of the late Archean Hamersley Basin, Western Australia. Org. Geochem. 34, 1161–1175.

Brocks, J.J., Love, G.D., Summons, R.E., Knoll, A.H., Logan, G.A., Bowden, S.A., 2005. Biomarker evidence for green and purple sulphur bacteria in a stratified Palaeoproterozoic sea. Nature 437, 866–870.

Brooks, J.D., Gould, K., Smith, J.W., 1969. Isoprenoid Hydrocarbons in Coal and Petroleum. Nature 222, 257–259.

Butterfield, N.J., 2003. Exceptional Fossil Preservation and the Cambrian Explosion. Integr. Comp. Biol. 43, 166–177.

Canfield, D.E., 1998. A new model for Proterozoic ocean chemistry. Nature 396, 450–453.

Canfield, D.E., 2005. The early history of atmospheric oxygen: Homage to Robert M. Garrels. Annu. Rev. Earth Pl. Sci. 33, 1–36.

Crick, I.H., 1992. Petrological and maturation characteristics of organic matter from the Middle Proterozoic McArthur Basin. Australia. Aust. J. Earth Sci. 39, 501–519.

Cui, J., 2011. Comparison of Multiple Occurrence Biomarkers of Core and Outcrop in Gaoyuzhuang and Hongshuizhuang Fm. Jibei Sag. Acta Sedimentol. Sin. 29, 593–598 in Chinese.

Cui, X., Liu, X.-L., Shen, G., Ma, J., Husain, F., Rocher, D., Zumberge, J., Bryant, D., Summons, R., 2020. Niche expansion for phototrophic sulfur bacteria at the Proterozoic-Phanerozoic transition. P. Natl. Acad. Sci. USA 117, 1–8.

Douglas, A.G., B.J., M., 1965. Sulfur: role in genesis of petroleum. Science 147, 499–501.

Dutkiewicz, A., Volk, H., Ridley, J., George, S.C., 2004. Geochemistry of oil in fluid inclusions in a middle Proterozoic igneous intrusion: implications for the source of hydrocarbons in crystalline rocks. Org. Geochem. 35, 937–957.

Dutta, S., Greenwood, P.F., Brocke, R., Schaefer, R.G., Mann, U., 2006. New insights into the relationship between Tasmanites and tricyclic terpenoids. Org. Geochem. 37, 117–127.

Ekweozor, C.M., 1984. Tricyclic terpenoid derivatives from chemical degradation reactions of asphaltenes. Org. Geochem. 6, 51–61.

Farrimond, P., Telnæs, N., 1996. Three series of rearranged hopanes in Toarcian sediments (northern Italy). Org. Geochem. 25, 165–177.

French, K.L., Hallmann, C., Hope, J.M., Schoon, P.L., Zumberge, J.A., Hoshino, Y., Peters, C.A., George, S.C., Love, G.D., Brocks, J.J., Buick, R., Summons, R.E., 2015. Reappraisal of hydrocarbon biomarkers in Archean rocks. P. Natl. Acad. Sci. USA 112, 5915–5920.

Goossens, H., de Leeuw, J.W., Schenck, P.A., Brassell, S.C., 1984. Tocopherols as likely precursors of pristane in ancient sediments and crude oils. Nature 312, 440–442.

Greenwood, P.F., Arouri, K.R., George, S.C., 2000. Tricyclic terpenoid composition of tasmanites kerogen as determined by pyrolysis GC-MS. Geochim. Cosmochim. Acta 64, 1249–1263.

Grice, K., Schouten, S., Nissenbaum, A., Charrach, J., Sinninghe Damsté, J.S., 1998. Isotopically heavy carbon in the C21 to C25 regular isoprenoids in halite-rich deposits from the Sdom Formation, Dead Sea Basin. Israel. Org. Geochem. 28, 349–359.

Hatch, J.R., Leventhal, J.S., 1992. Relationship between inferred redox potential of the depositional environment and geochemistry of the Upper Pennsylvanian (Missourian) Stark Shale Member of the Dennis Limestone, Wabaunsee County, Kansas, U.S.A. Chem. Geol. 99, 65–82.

Hedberg, H.D., 1968. Significance of High-Wax Oils with Respect to Genesis of Petroleum. AAPG Bull. 52, 736–750.

Hills, I.R., Whitehead, E.V., Anders, D.E., Cummins, J.J., Robinson, W.E., 1966. An optically active triterpane, gammacerane in Green River, Colorado, oil shale bitumen. Chem. Commun. 20, 752–754.

Holland, H.D., 1984. The chemical evolution of the atmosphere and oceans. Princeton Univ. Press, Princeton, NJ.

Holland, H.D., 2006. The oxygenation of the atmosphere and oceans. Philos. T. R. Soc. B. 361, 903–915.

Hughes, W.B., Holba, A.G., Dzou, L.I.P., 1995. The ratios of dibenzothiophene to phenanthrene and pristane to phytane as indicators of depositional environment and lithology of petroleum source rocks. Geochim. Cosmochim. Acta 59, 3581–3598.

Jacob, H., 1989. Classification, structure, genesis and practical importance of natural solid oil bitumen ("migrabitumen"). Int. J. Coal Geol. 11, 65–79.

Jarrett, A.J.M., Schinteie, R., Hope, J.M., Brocks, J.J., 2013. Micro-ablation, a new technique to remove drilling fluids and other contaminants from fragmented and fissile rock material. Org. Geochem. 61, 57–65.

Jarrett, A.J.M., Cox, G.M., Brocks, J.J., Grosjean, E., Boreham, C.J., Edwards, D.S., 2019. Microbial assemblage and palaeoenvironmental reconstruction of the 1.38 Ga Velkerri Formation, McArthur Basin, northern Australia. Geobiology 17, 360–380.

Kelly, A.E., Love, G.D., Zumberge, J.E., Summons, R.E., 2011. Hydrocarbon biomarkers of Neoproterozoic to Lower Cambrian oils from eastern Siberia. Org. Geochem. 42, 640–654.

Kenig, F., 2000. C16–C29 homologous series of monomethylalkanes in the pyrolysis products of a Holocene microbial mat. Org. Geochem. 31, 237–241.

Kenig, F., Sinninghe Damsté, J.S., de Leeuw, J.W., Hayes, J.M., 1994. Molecular palaeontological evidence for food-web relationships. Naturwissenschaften 81, 128–130.

Kissin, Y.V., 1987. Catagenesis and composition of petroleum: Origin of n-alkanes and isoalkanes in petroleum crudes. Geochim. Cosmochim. Acta 51, 2445–2457.

Kolaczkowska, E., Slougui, N.-E., Watt, D.S., Maruca, R.E., Michael Moldowan, J., 1990. Thermodynamic stability of various alkylated, dealkylated and rearranged 17α- and 17β-hopane isomers using molecular mechanics calculations. Org. Geochem. 16, 1033–1038.

Kvalheim, O.M., Christy, A.A., Telnæs, N., Bjørseth, A., 1987. Maturity determination of organic matter in coals using the methylphenanthrene distribution. Geochim. Cosmochim. Acta 51, 1883–1888.

Lee, C., Love, G.D., Jahnke, L.L., Kubo, M.D., Des Marais, D.J., 2019. Early diagenetic sequestration of microbial mat lipid biomarkers through covalent binding into insoluble macromolecular organic matter (IMOM) as revealed by sequential chemolysis and catalytic hydropyrolysis. Org. Geochem. 132, 11–22.

Lee, C., Love, G.D., Jahnke, L.L., Kubo, M.D., Des Marais, D.J., 2021. Diagenetic transformations and preservation of free and bound lipids in a hypersaline microbial mat from Guerrero Negro, Baja California Sur. Mexico. Org. Geochem. 153, 104196.

Li, C., Peng, P.a., Sheng, G., Fu, J., Yan, Y., 2001. A biomaekers study of Paleo- to Neo-proterozoic (1.8~0.85 Ga) sediments from the Jixian strata section, North China. Front. Earth Sci. 8, 463–462 (in Chinese).

Li, C., Peng, P.A., Sheng, G., Fu, J., Yan, Y., 2003. A molecular and isotopic geochemical study of Meso- to Neoproterozoic (1.73–0.85 Ga) sediments from the Jixian section, Yanshan Basin, North China. Precambrian Res. 125, 337–356.

Li, C., Love, G.D., Lyons, T.W., Fike, D.A., Sessions, A.L., Chu, X., 2010. A stratified redox model for the Ediacaran ocean. Science 328, 80–83.

Li, M., Wang, T., Zhong, N., Zhang, W., Sadik, A., Li, H., 2013. Ternary diagram of fluorenes, dibenzothiophenes and dibenzofurans: Indicating depositional environment of crude oil source rocks. Energ. Explor. Exploit. 31, 569–588.

Logan, G.A., Hayes, J.M., Hieshima, G.B., Summons, R.E., 1995. Terminal Proterozoic reorganization of biogeochemical cycles. Nature 376, 53–56.

Love, G.D., Snape, C.E., Carr, A.D., Houghton, R.C., 1995. Release of covalently-bound alkane biomarkers in high yields from kerogen via catalytic hydropyrolysis. Org. Geochem. 23, 981–986.

Love, G.D., Bowden, S.A., Jahnke, L.L., Snape, C.E., Campbell, C.N., Day, J.G., Summons, R.E., 2005. A catalytic hydropyrolysis method for the rapid screening of microbial cultures for lipid biomarkers. Org. Geochem. 36, 63–82.

Love, G., Stalvies, C., Grosjean, E., Meredith, W., Snape, C., 2008. Analysis of molecular biomarkers covalently bound within Neoproterozoic sedimentary kerogen. From Evolution to Geobiology: Research Questions Driving Paleontology at the Start of a New Century 14, 67–83.

Luo, Q., George, S.C., Xu, Y., Zhong, N., 2016. Organic geochemical characteristics of the Mesoproterozoic Hongshuizhuang Formation from northern China: Implications for thermal maturity and biological sources. Org. Geochem. 99, 23–37.

Luo, G., Hallmann, C., Xie, S., Ruan, X., Summons, R.E., 2015. Comparative microbial diversity and redox environments of black shale and stromatolite facies in the Mesoproterozoic Xiamaling Formation. Geochim. Cosmochim. Acta 151, 150–167.

Luo, Q., Zhong, N., Qin, J., Li, K., Zhang, Y., Wang, Y., Ma, L., 2014. Thucholite in Mesoproterozoic shales from northern north China: Occurrence and indication for thermal maturity. Int. J. Coal Geol. 125, 1–9.

Lyons, T.W., Werne, J.P., Hollander, D.J., Murray, R.W., 2003. Contrasting sulfur geochemistry and Fe/Al and Mo/Al ratios across the last oxic-to-anoxic transition in the Cariaco Basin. Venezuela. Chem. Geol. 195, 131–157.

Lyons, T.W., Anbar, A.D., Severmann, S., Scott, C., Gill, B.C., 2009. Tracking Euxinia in the Ancient Ocean: A Multiproxy Perspective and Proterozoic Case Study. Annu. Rev. Earth Pl. Sc. 37, 507–534.

Miao, L., Moczydowska, M., Zhu, M., 2021. A diverse organic-walled microfossil assemblage from the Mesoproterozoic Xiamaling Formation. North China. Precambrian Res. 360, 106235.

Moldowan, J.M., Fago, F.J., Carlson, R.M.K., Young, D.C., van Duyne, G., Clardy, J., Schoell, M., Pillinger, C.T., Watt, D.S., 1991. Rearranged hopanes in sediments and petroleum. Geochim. Cosmochim. Acta 55, 3333–3353.

Mukhopadhyay, P.K., Wade, J.A., Kruge, M.A., 1995. Organic facies and maturation of Jurassic/Cretaceous rocks, and possible oil-source rock correlation based on pyrolysis of asphaltenes, Scotia Basin. Canada. Org. Geochem. 22, 85–104.

Nguyen, K., Love, G.D., Zumberge, J.A., Kelly, A.E., Owens, J.D., Rohrssen, M.K., Bates, S.M., Cai, C., Lyons, T.W., 2019. Absence of biomarker evidence for early eukaryotic life from the Mesoproterozoic Roper Group: Searching across a marine redox gradient in mid-Proterozoic habitability. Geobiology 17, 247–260.

Ourisson, G., 1994. Biomarkers in the Proterozoic record. In Early Life on Earth. Columbia University Press, New York. 84 (ed. S. Bengtson), 259–269.

Pawlowska, M.M., Butterfield, N.J., Brocks, J.J., 2013. Lipid taphonomy in the Proterozoic and the effect of microbial mats on biomarker preservation. Geology 41, 103–106.

Peters, K.E., Walters, C.C., Moldowan, J.M., 2005. The Biomarker Guide: Biomarkers and Isotopes in Petroleum Exploration and Earth History. seconded. vol 2 Cambridge University Press, Cambridge.

Peters, K.E., Moldowan, J.M., 1993. The Biomarker Guide: Interpreting Molecular Fossils in Petroleum and Ancient Sediments. Prentice Hall, Englewood Cliffs, New Jersey.

Planavsky, N.J., McGoldrick, P., Scott, C.T., Li, C., Reinhard, C.T., Kelly, A.E., Chu, X., Bekker, A., Love, G.D., Lyons, T.W., 2011. Widespread iron-rich conditions in the mid-Proterozoic ocean. Nature 477, 448–451.

Poulton, S.W., Canfield, D.E., 2011. Ferruginous Conditions: A Dominant Feature of the Ocean through Earth`s History. Elements 7, 107–112.

Poulton, S.W., Fralick, P.W., Canfield, D.E., 2004. The transition to a sulphidic ocean approximately 1.84 billion years ago. Nature 431, 173–177.

Poulton, S., Fralick, P., Canfield, D., 2010. Spatial variability in oceanic redox structure 1.8 billion years ago. Nature Geosci. 3, 486–490.

Radke, M., Welte, D.H., Willsch, H., 1982a. Geochemical study on a well in the Western Canada Basin: relation of the aromatic distribution pattern to maturity of organic matter. Geochim. Cosmochim. Acta 46, 1–10.

Radke, M., Leythaeuser, D., Teichmüller, M., 1984. Relationship between rank and composition of aromatic hydrocarbons for coals of different origins. Org. Geochem. 6, 423–430.

Radke, M., Welte, H., 1983. The Methylphenanthrene Index (MPI): A maturity parameter based on aromatic hydrocarbons. Proceedings of the International Meeting on Organic Geochemistry 10, 504–512.

Radke, M., Willsch, H., Leythaeuser, D., Teichmüller, M., 1982b. Aromatic components of coal: relation of distribution pattern to rank. Geochim. Cosmochim. Acta 46, 1831–1848.

Rasmussen, B., Fletcher, I.R., Brocks, J.J., Kilburn, M.R., 2008. Reassessing the first appearance of eukaryotes and cyanobacteria. Nature 455, 1101–1104.

Robison, C.R., Smith, M.A., Royle, R.A., 1999. Organic facies in Cretaceous and Jurassic hydrocarbon source rocks, Southern Indus basin. Pakistan. Int. J. Coal Geol. 39, 205–225.

Rohmer, M., Bisseret, P., Neunlist, S., 1992. The hopanoids, prokaryotic triterpenoids and precursors of ubiquitous molecular fossils. In Biological Markers in Sediments and Petroleum (eds. J. M. Moldowan, P. Albrecht, and R. P. Philp), Prentice Hall, New York., 1–17.

Scott, C., Lyons, T.W., Bekker, A., Shen, Y., Poulton, S.W., Chu, X., Anbar, A.D., 2008. Tracing the stepwise oxygenation of the Proterozoic ocean. Nature 452, 456–459.

Shen, Y., Canfield, D.E., KNOLL, A.H., 2002. Shen, Y., Canfield, D. E. & Knoll, A. H. Middle Proterozoic ocean chemistry: Evidence from the McArthur Basin, northern Australia. Am. J. Sci. 302, 81–109.

Shen, Y., Thiel, V., Suarez-Gonzalez, P., Rampen, S., Reitner, J., 2020. Sterol preservation in hypersaline microbial mats. Biogeosciences 17, 649–666.

Sherman, L.S., Waldbauer, J.R., Summons, R.E., 2007. Improved methods for isolating and validating indigenous biomarkers in Precambrian rocks. Org. Geochem. 38, 1987–2000.

Shiea, J., Brassell, S.C., Ward, D.M., 1990. Mid-chain branched mono- and dimethyl alkanes in hot spring cyanobacterial mats: A direct biogenic source for branched alkanes in ancient sediments? Org. Geochem. 15, 223–231.

Simoneit, B.R.T., Leif, R.N., Neto, F.R.D.A., Azevedo, D.A., Pinto, A.C., Albrecht, P., 1990. On the presence of tricyclic terpane hydrocarbons in permian tasmanite algae. Naturwissenschaften 77, 380–383.

Summons, R.E., Brassell, S.C., Eglinton, G., Evans, E., Horodyski, R.J., Robinson, N., Ward, D.M., 1988a. Distinctive hydrocarbon biomarkers from fossiliferous sediment of the Late Proterozoic Walcott Member, Chuar Group, Grand Canyon. Arizona. Geochim. Cosmochim. Acta 52, 2625–2637.

Summons, R.E., Jahnke, L.L., Hope, J.M., Logan, G.A., 1999. 2-Methylhopanoids as biomarkers for cyanobacterial oxygenic photosynthesis. Nature 400, 554–557.

Summons, R.E., Powell, T.G., 1986. Chlorobiaceae in Palaeozoic seas revealed by biological markers, isotopes and geology. Nature 319, 763–765.

Summons, R.E., Powell, T.G., Boreham, C.J., 1988b. Petroleum geology and geochemistry of the Middle Proterozoic McArthur Basin, Northern Australia: III. Composition of extractable hydrocarbons. Geochim. Cosmochim. Acta 52, 1747–1763.

Sun, S., Wang, T., 2016. Meso-Neoproterozoic geology and oil and gas resources in east China. Science Press, Beijing (in Chinese).

Takishita, K., Chikaraishi, Y., Tanifuji, G., et al., 2017. Microbial eukaryotes that lack sterols. J. Eukaryot. Microbiol. 64, 897–900.

Talbot, H.M., Summons, R.E., Jahnke, L.L., Cockell, C.S., Rohmer, M., Farrimond, P., 2008. Cyanobacterial bacteriohopanepolyol signatures from cultures and natural environmental settings. Org. Geochem. 39, 232–263.

Tegelaar, E.W., de Leeuw, J.W., Derenne, S., Largeau, C., 1989. A reappraisal of kerogen formation. Geochim. Cosmochim. Acta 53, 3103–3106.

Teichmuller, M., 1988. Mineral-Bituminous Groundmass. Minutes of the Meeting of the International Committee for Coal Petrologists, Commission II, Aachen, W. Germany.

Ten Haven, H.L., de Leeuw, J.W., Rullkötter, J., Damsté, J.S.S., 1987. Restricted utility of the pristane/phytane ratio as a palaeoenvironmental indicator. Nature 330, 641–643.

Tian, S., 1996. Stratigraphy (lithostratic) of the municipality of Tianjin. China University of Geosciences Press, Wuhan (in Chinese).

Wang, T., Han, K., 2011. On Meso-Neoproterozoic primary petroleum resources. Acta Petrol. Sin. 31, 1–7 in Chinese.

Wang, L., Li, B., 1993. Sedimentary sequences and source beds in the Xiamaling Formation in Northwestern Hebei. Sediment. Facies Palaeogeog. 13, 38–45 in Chinese.

Wang, T.G., Simoneit, B.R.T., 1995. Tricyclic terpanes in Precambrian bituminous sandstone from the eastern Yanshan region, North China. Chem. Geol. 120, 155–170.

Wang, X., Yuan, X., 2019. A molecular window to the primeval world. Chinese Sci. Bull. 64, 2279–2284 in Chinese.

Wang, X., Zhao, W., Zhang, S., Wang, H., Su, J., Canfield, D.E., Hammarlund, E.U., 2018. The aerobic diagenesis of Mesoproterozoic organic matter. Sci. Rep. 8, 13324.

Xiao, H., Li, M., Liu, J., Mao, F., Cheng, D., Yang, Z., 2019a. Oil-oil and oil-source rock correlations in the Muglad Basin, Sudan and South Sudan: New insights from molecular markers analyses. Mar. Petrol. Geol. 103, 351–365.

Xiao, H., Li, M., Wang, W., You, B., Liu, X., Yang, Z., Liu, J., Chen, Q., Uwiringiyimana, M., 2019b. Identification, distribution and geochemical significance of four rearranged hopane series in crude oil. Org. Geochem. 138, 103929.

Xiao, H., Li, M., Yang, Z., Zhu, Z., 2019c. The distribution patterns and geochemical implication of C19–C23 tricyclic terpanes in source rocks and crude oils occurred in various depositional environment. Acta Geochem. 48, 161–170 in Chinese.

Xiao, H., Li, M., Wang, T., You, B., Leng, J., Han, Q., Ran, Z., Wang, X., Gao, Z., 2021a. Four series of rearranged hopanes in the Mesoproterozoic sediments. Chem. Geol. 573, 120210.

Xiao, H., Wang, T., Li, M., You, B., Zhu, Z., 2021b. Extended series of tricyclic terpanes in the Mesoproterozoic sediments. Org, Geochem, p. 104245.

Yan, Y., Liu, Z., 1998. The relationship between biocommunities and Paleoenvironments in Changcheng Period of the Yanshan Basin, North China. Acta MicroPaleontologica Sinica 15, 249–266 in Chinese.

Zhang, S., Huang, H., 2005. Geochemistry of Palaeozoic marine petroleum from the Tarim Basin, NW China: Part 1. Oil family classification. Org. Geochem. 36, 1204–1214.

Zhang, S., Zhang, B., Bian, L., Jin, Z., Wang, D., Chen, J., 2007. The oil shale formed by the accumulation of the red algae more than 800 million years ago in Xiamaling Formation. Sci. China (Seri. D): Earth Sci. 37, 636–643 in Chinese.

Zhang, S., Wang, X., Hammarlund, E., Wang, H., Costa, M., Bjerrum, C., Connelly, J., Zhang, B., Bian, L., Canfield, D., 2015. Orbital forcing of climate 1.4 billion years ago. P. Natl. Acad. Sci. USA 112, 1406–1413.

Zhang, S., Wang, X., Wang, H., Bjerrum, C., Hammarlund, E., Costa, M., Connelly, J., Zhang, B., Su, J., Canfield, D., 2016. Sufficient oxygen for animal respiration 1,400 million years ago. P. Natl. Acad. Sci. USA 113, 201523449.

Zumberge, J.E., 1987. Prediction of source rock characteristics based on terpane biomarkers in crude oils: A multivariate statistical approach. Geochim. Cosmochim. Acta 51, 1625–1637.